# Rising Temperatures, Rising Risks: Changes in Chinese Children's Ambient Heat Exposure between 1990 and 2020

Kai Feng, Marco M. Laghi, Jere R. Behrman, Emily Hannum, and Fan Wang*

July 21, 2025

Please click here for latest version of the paper.

**Abstract**

The frequency and intensity of heat waves are increasing as the earth's climate warms, but how these trends translate to changes in children's ambient heat exposure is not well-established. Existing studies often measure heat exposure using person-time units, which overlook variations in risk levels and exposure durations. Our study addresses this gap by developing a double-dual-distributional (DDD) framework to assess heat exposure among 250 million children in China from 1990 to 2020. We found that children's average annual exposure to moderate or stronger heat stress increased by 238 hours, and the proportion experiencing over 18 weeks of such stress more than doubled. This framework highlights that both rising temperatures and shifts in child population distributions contribute to increased heat exposure, offering new insights for mitigating climate-related risks to children's health.

**Keywords**: Extreme heat, children, China, geographic distribution of children

*Kai Feng: Department of Sociology and Population Studies Center, University of Pennsylvania, Philadelphia, Pennsylvania, USA; Marco M. Laghi: Department of Sociology, New York University, New York, NY, USA; Center for Applied Social and Economic Research, NYU Shanghai, Shanghai, China; Jere R. Behrman: Departments of Economics and Sociology and Population Studies Center, University of Pennsylvania, Philadelphia, Pennsylvania, USA; Emily Hannum: Department of Sociology and Population Studies Center, University of Pennsylvania, Philadelphia, Pennsylvania, USA; Fan Wang: Department of Economics, University of Houston, Houston, Texas, USA. This paper is supported by National Science Foundation Grants 1756738 and 2230615.

# 1 Introduction

Extreme heat exposure is a significant and growing threat to human health and welfare (Carleton and Hsiang 2016; Ebi et al. 2021; Gasparrini et al. 2015; Kovats and Hajat 2008; Mora et al. 2017), with research increasingly highlighting its disproportionate impacts on vulnerable populations (Harrington et al. 2016; Hsu et al. 2021; Li et al. 2016; Mitchell and Chakraborty 2015; Xi et al. 2024). Children are particularly susceptible to the detrimental effects of heat exposure because of their lower ability to self-thermoregulate, impaired thirst sensation, and impaired glomerular filtration rates (Connon and Dominelli 2022a, 2022b; Park, Behrer, and Goodman 2021; Prentice et al. 2024; Zivin and Shrader 2016). Studies have shown that extreme heat directly impacts children by undermining their nutrition (Baker and Anttila-Hughes 2020), impairing cognition and skill development (Park, Behrer, and Goodman 2021), and escalating rates of heat-related illnesses and mortality (Helldén et al. 2021; Zivin and Shrader 2016). The negative effects of heat exposure can begin as early as the prenatal stage (Edwards, Saunders, and Shiota 2003). Research has linked high temperatures to increased instances of preterm births and low birth weights (Grace et al. 2015; Liu et al. 2022; Ren et al. 2023). Additionally, extreme heat indirectly affects children by exacerbating droughts and associated food insecurity (Chavez et al. 2015; Cooper et al. 2019; Sun et al. 2024), intensifying tropical disasters (Grinsted, Moore, and Jevrejeva 2013; Walsh et al. 2016), facilitating the spread of infectious diseases (Mahon et al. 2024; Mora et al. 2022; Onozuka and Hashizume 2011; Xu, Liu, et al. 2014) , and heightening the risk of violent conflicts (Akresh 2016; Hsiang, Burke, and Miguel 2013).

Climatic change has both prolonged and intensified extreme heat exposures (Jones et al. 2015; Li and Zha 2020; Sun et al. 2022; Sun et al. 2014; Tuholske et al. 2021). Projections suggest a significant rise in the burden of heat exposures on populations, a trend attributed to both climatic changes and the increased populations exposed to these changes (Jones et al. 2018; Liu et al. 2017). Yet, only a few studies focus on measuring exposure to heat among the child population despite the great vulnerability of children to heat exposures (UNICEF 2021, 2022). While UNICEF 2022 offers one form of evaluation of child heat exposure, their analysis has limitations in using nationally aggregated total population data to infer the distribution of children. Our contribution in comparison is the explicit use of intra-national child population distributional data. In addition, the prevalent approach in studies that measure general population heat burdens is to measure the total burden in person-time units, calculated by multiplying

the total population by the time that the average person experiences heat exposures above designated thresholds (Jones et al. 2015; Liu et al. 2017; Sun et al. 2022; Tuholske et al. 2021). While useful for capturing aggregate exposures, this method overlooks heterogeneities in intensity, duration, and risk levels, and obscures distributional inequalities by assuming uniform exposures across space, time, and demographic groups. Further, an overreliance on person-time units can be misleading in contexts of population decline, where aggregate exposure may decrease even as individual-level risk remains high. This limitation is especially relevant for assessing heat exposure of the child population, which is shrinking in most countries due to declining fertility.

Using the case of China—home to approximately 253.3 million children ages 0–14 in 2020 (National Bureau of Statistics of China 2021)—this paper provides the first empirical evidence on how heat exposures, at varying intensity and duration thresholds, have been changing for children in recent decades. We propose a convenient, low-data-demand framework for measuring the share of children at risk of extreme heat exposures. Using what we call the *double-dual-distributional (DDD)* framework, we measured population-level child-heat-exposure changes by jointly considering two types of geospatial and temporal distributions—that of perceived temperatures and that of child populations—and two types of heat-exposure thresholds—for intensity (heat-stress levels) and duration (hourly exceedance). In this framework, we compute a *Share of Time for the Average Child* (STAC) statistic, measuring the share of time exposed to extreme heat for the average child at any given heat threshold, and a *Share Exposed by Intensity and Duration Thresholds* (SEIDT) statistic, measuring the share of children exposed to extreme heat by differing intensity and duration thresholds.

We accomplished this by linking county-level child-population data to the hourly Universal Thermal Climate Index (UTCI), a physiologically based human-thermal-stress index that quantifies perceived temperature by integrating air temperature, humidity, wind speed, and mean radiant temperature (Blazejczyk et al. 2013; Bröde et al. 2012; Jendritzky, Dear, and Havenith 2012), across two censuses spanning 30 years (1990-2020). Specifically, we merged child populations from 2,369 (year 1990) and 2,853 (year 2020) county-level administrative units with 15,432 grid points ($0.25^\circ \times 0.25^\circ$ spatial resolution) of hourly UTCI data that overlap with the administrative boundary of mainland China. The wide dispersion of child populations across counties and the limited geographic expanse of most Chinese counties allows for the construction of granular child-population-weighted national and regional UTCI-based heat exposure

statistics. Additionally, previous research highlights that heat effects depend on local population susceptibility, local climatology, and local adaptation. To capture these variations, we provide both national and regional level results (Arbuthnott et al. 2016; Guo et al. 2014).

We found substantial increases in the average heat-stress exposure for children and in the share of children at risk. Specifically, the average child was exposed to moderate or higher levels of heat stress for an additional 238 hours in 2020 in comparison to 1990. The share of children subjected to over 18 weeks per year of such heat stress more than doubled, increasing from 6.7% to 13.7%. We also found that approximately half of the overall change in child heat-stress exposures between 1990 and 2020 was driven by heat increases, and the rest was driven by cross-location shifts in the child population towards locations that had higher heat stress, illustrating the importance of *both* heat patterns *and* child population distributions. Finally, we highlighted significant regional disparities: In Eastern China, China's most-developed region, there was a marked increase in the duration of children's heat exposure from 1990 to 2020, even though the exposure levels were already high in 1990. Conversely, the Central region, which had comparable exposure levels as the Eastern region in 1990, experienced only a minimal increase in aggregate child-heat exposures from 1990 to 2020.

## 2 Methods and Data

**Methods.** In this section, we summarize our *double-dual-distributional (DDD)* framework for measuring child population at risk of heat exposure. Within a particular span of time in a region, our DDD framework develops two statistics for heat exposure risks building on two types of distributions and two types of thresholds. The two distributions are the distribution of location-specific UTCI temperature and the distribution of location-specific population groups (e.g., children). The two thresholds are UTCI-based heat stress thresholds (intensity of exposure) for extreme heat exposure and time thresholds (duration of exposure) for the share of time exposed to extreme heat. The first risk statistic, STAC, captures the risk of extreme heat exposure facing the average child, measured in units of *share of time the average child* is exposed to extreme heat in a particular period. The second risk statistic, SEIDT, captures the distribution of risk among children, measured in units of the *share of child population exposed to extreme heat by different intensity and duration thresholds*. While the overall framework allows for the incorporation of additional heat exposure dimensions—such as the length of specific

heat spells—that would require dividing children into more granular cells of exposure experiences. Therefore, we focused on heat-intensity and overall-time-duration as two first-order dimensions of heat exposure experiences.

Existing studies that consider population heat exposures have computed changes in heat exposure in total person-time units for a particular region or country. The person-days of heat exposure in a place at time t can be computed, for example, by multiplying the days during which the maximum temperature exceeds a threshold level with the total population residing in a place at time t. Aggregate person-time statistics have two limitations. First, when comparing exposures over time, aggregate person-time statistics will capture changes in aggregate population size over time in addition to changes in average heat exposure burdens. As countries have experienced diverse patterns of declining and increasing child populations in recent decades (Hannum, Kim, and Wang 2024), the resultant person-time estimates may not reflect average child heat exposure experiences. Second, the person-time aggregate provides a single statistic of exposure for a region or country, overlooking the within-region or within-country heterogeneities in ambient exposure changes across populations residing in locations with differing climatic-change experiences. In addition to considering both climatic and population distributions, as done in person-time statistics, our DDD framework captures heterogeneities across time and space by measuring changes in the percentages of children experiencing different intensities of heat stress for different durations over time.

In the closest-related work, UNICEF estimated for each country the number of children at risk of heat exposure based on the aggregate national population share of children in 2020 (UNICEF 2022). Our framework is the first to compute population-level distributional changes in heat exposure for children over time. By providing—for the first time and in a large economy—measurements on changes in the shares of children at risk of the double-thresholds of heat exposure, our framework and empirical results complement and extend existing research that has shown negative effects of heat exposure on children.

We implemented our framework in the setting of China between 1990 and 2020. In this empirical application, we considered each span of time as one year, we approximated continuous-ambient-heat exposures based on hourly estimates of UTCI, and we approximated fine-grained measures of locations with counties (3rd-level administrative units) in China. Depending on the analysis, we consider all county-level administrative units in China, in a region of China, or in a province, and generate year-specific child-population-weighted heat distributions by sort-

ing counties along increasing levels of heat exposures and summing up the share of child population along this ascending heat gradient. We show in the Supplement Section B.2 that population data from more than 2,300 Chinese county-level administrative units and heat data from more than 15 thousand gridded UTCI data points that overlap with mainland China provide granular joint measurements of child population and heat data. For the exposure-intensity thresholds, we considered a range of UTCI thresholds but focused our analysis on key thresholds for extreme heat commonly used in the literature. For exposure-duration thresholds, we considered different shares of time during the course of a year that a child is exposed to UTCI temperatures above the intensity-thresholds considered. Our method is also straightforward to implement in other settings where tabular population data at a relatively fine-grained level and location-specific climate data are available.

**Data.** To measure heat, we used the fifth generation of the European Centre for Medium-Range Weather Forecasts (ECMWF) atmospheric reanalyses of the global climate: the ERA5-HEAT dataset (Napoli 2020). ERA5-HEAT provides hourly data on UTCI with a spatial resolution of 0.25 degrees. The UTCI index provides an integrative measure of the perceived thermal stress on the human body, taking into account factors such as air temperature, humidity, wind speed, and radiant heat (Bröde et al. 2012; Jendritzky, Dear, and Havenith 2012; Jendritzky and Höppe 2017). When UTCI is between 26 °C and 32 °C, it indicates moderate-heat stress on the human body, signifying warm conditions where individuals may start to feel uncomfortable, especially if engaging in physical activity. As the UTCI value increases, the level of thermal stress on the human body intensifies. UTCI values between 32 °C and 38 °C indicate strong-heat stress, whereas UTCI values between 38 °C and 46 °C indicate very-strong-heat stress (Bröde et al. 2012). We utilized these UTCI stress categories in this study.

For population data, we utilized Chinese-census data for the years 1990 and 2020 (All China Market Research Ltd 2022; Beijing Hua tong ren shi chang xin xi you xian ze ren gong si 2005a, 2005b; China Data Lab 2020). County-level child population data and county-level administrative boundary files were extracted and used to construct ages 0–14 populations by county. For regional analysis, we considered the child population and UTCI distributions within each one of the four recognized economic regions of China (National Bureau of Statistics of China 2011).

## 3 Results

**Increase in the Share of Time Exposed to Heat for Average Child (STAC).** Figure 1 depicts the *percentage-point changes* (Panel a) and *percentage changes* (Panel b) in the STAC statistics, which measure the average share of time in ambient-heat stress for the average child from 1990 to 2020. The three-colored backgrounds in this figure reflect the heat-stress levels associated with different UTCI thresholds. UTCI above 26 °C marks the beginning of moderate heat stress, in which healthy individuals may begin to feel heat discomfort, and vulnerable populations like children may start experiencing elevated health risks, especially with prolonged exposure (Blazejczyk et al. 2013; Di Napoli, Pappenberger, and Cloke 2018; Romaszko et al. 2022). UTCI above 32 °C and above 38 °C mark the onset of strong and very strong heat stress, respectively, when health risks become more serious and widespread (Blazejczyk et al. 2013; Di Napoli, Pappenberger, and Cloke 2018; Romaszko et al. 2022).

We present changes in STAC statistics using three different within-year time frames: all annual hours, daytime hours (6 a.m.–10 p.m.), and hours during April to September, as the hot months of the year. Across the three time-frame specifications, the average child's share of time in heat stress increased in China from 1990 to 2020 across all UTCI heat thresholds. The largest percentage-point change (Figure 1 Panel a) occurred when considering only hours in hot months, followed by daytime hours, and then all annual hours. The percentage changes (Figure 1 Panel b) largely overlapped across the three time-frame specifications.

When all hours were considered, the average child in China experienced 20.1% of her total hours in 1990 at-or-above 26 °C UTCI (at-least-moderate heat stress). By 2020, this percentage increased to 22.8%, representing a 2.7 percentage-point (Figure 1 Panel a) and 13.5% increase in annual average exposure duration (Figure 1 Panel b), which corresponded to an average increase over 30 years of 238 hours of additional moderate-or-stronger heat-stress exposure.

Across all heat-stress thresholds, the average child's share of time at risk of heat stress increased. While the percentage-point increases were smaller at higher-heat thresholds, the percentage increases in the average child shares of time exposed to UTCI thresholds between 26 °C to 40 °C were similar and ranged between 14% and 18%. For example, the average duration of children's exposure to UTCI at-or-above 32 °C increased by 1.1 percentage points, reflecting a 14.7% rise as compared to the levels observed in 1990. These results also indicated that approximately 40% (calculated as $1 - \frac{2.7-1.1}{2.7} \approx 0.4$) of the increase in average-heat exposure at the

26 °C threshold can be attributed to the escalation in exposure to strong-or-above heat stress exceeding the 32 °C threshold. Tables C.1 and C.2 in the online Appendix enumerate levels and changes for average child-heat exposure at additional UTCI thresholds.

**Increases in Shares of Children Exposed by Intensity and Duration Thresholds (SEIDT).** While the previous results focus on heat exposure for the average child in China, they do not provide information on how many children were increasingly at risk of ambient heat exposure. Therefore, given the changing distributions of heat and of children across counties in China, we computed the SEIDT statistics and examined whether the *percentages* of children most affected by heat stress also changed over time.

We computed the share of children at risk by jointly considering two thresholds of risks: a threshold for the level of heat-stress exposure (intensity) and a threshold for the share of annual hours (duration) exposed to heat stress above a particular threshold. Figure 2 presents results for combinations of selected thresholds for the duration of time exposed to heat stress (from 4% to 36%) and the intensity of heat stress (from above 26 °C to above 38 °C). Online Appendix Tables C.3 and C.4 provide tabulations at additional thresholds.

Exposure to at-least-some moderate-heat stress was nearly universal among children in China. In 1990 (Figure 2 Panel a) and 2020 (Figure 2 Panel b), respectively, 97.2% and 97.7% of children experienced at least 4% of their hours, or over 2 weeks, in moderate-or-stronger-heat stress (i.e. UTCI $\geqslant$ 26 °C). At longer durations of exposure to heat stress, the shares of affected children were lower.

The shares of children enduring prolonged exposure to heat stress increased substantially from 1990 to 2020. In 1990, 6.7% of children (21.0 million) experienced moderate or stronger heat stress for more than 36% of their total hours, or equivalently, for over 16 weeks. By 2020, this share rose to 13.7% (34.7 million), marking an increase of 7.0 percentage points (Figure 2 Panel c) or 106%. In other words, the shares of children experiencing *at-least* moderate-heat stress for *at least* 32% of their total hours in 2020 more than doubled compared to 1990.

Similar increases in the shares of children experiencing heat stress were observed along a frontier of higher (or lower) heat-stress intensity and lower (or higher) duration combinations. For example, 11.2% of children (35.1 million) had at least 12% of their total hours, or 6 weeks at strong-heat stress or above (UTCI$\geqslant$ 32 °C). This number rose to 18.6% (47.1 million) in 2020, representing a 7.4 percentage-point or 66.3% increase.

Especially alarming were rapid increases in the shares of children at risk for very-strong-heat stress, emerging first for low duration of exposure. In particular, the shares of children experiencing at least 4% of their total hours at very-strong-heat stress (UTCI $\geqslant$ 38 °C) increased from 0.1% (0.3 million) to 1.8% (4.6 million). While the shares of children exposed to these extreme-risk levels remained small, these increases represented approximately an 18-fold jump in the shares of children at these high-exposure-risk levels.

**Decomposing the Contributions of Changes in Climate and Population.** Our decomposition analysis illustrates the extent to which changes in children's heat exposures over time can be attributed to shifts in the child population distribution, or due to changes in UTCI driven by meteorological changes. In this calculation, we computed counterfactual STAC statistics after altering one distribution (either children's population or UTCI) to 2020 levels while keeping the other constant at 1990 levels, without modeling mechanisms of change.

Figure 3 demonstrates that the increase in the average child's heat-stress exposure from 1990 to 2020 resulted from both climatic change and shifts in children's population distribution. For at-least-strong (UTCI $\geqslant$ 32 °C) and at-least-moderate (UTCI $\geqslant$ 26 °C) heat-stress levels, child population distributional shifts accounted for 48% and 50% of the actual change, respectively. UTCI distributional shifts accounted for 42% and 40% of the actual changes, respectively. The remaining residual changes were due to interactions between shifts in climatic and population distributions.

While both population distributional changes and climatic changes contributed to the rise in the average-child's heat-stress exposures, regional decomposition analysis showed varying contributions within regions. Specifically, changes in the population distribution accounted for about 1/3 of the exposure shifts in the Eastern region and less than 1/5 in the Northeastern region. This suggests that cross-region shifts in children's distribution, for example, due to migration to the Eastern region or fertility decline in the Northeastern region, contributed significantly to the national-population-decomposition results. Appendix Table C.5 provides additional details on regional-decomposition results.

Figure 3 also indicates that at higher-UTCI thresholds, the influence of changes in population distributions diminished. Nationally, the contribution of population distributions to heat-stress exposure declined with increasing-heat thresholds, from 50% at the 26 °C UTCI threshold to 39% at the 36 °C UTCI threshold. Similarly, the contribution of changes in population

distributions declined from 38% to 19% in the Eastern region and from 16% to 5% in the Northeastern region over the same sets of UTCI-threshold increments. This suggests that the rise in more-extreme heat exposures was primarily a result of climatic changes, rather than shifts in the geographic distribution of children toward already hotter areas. One possible explanation for this trend is the demographic transition in many highly developed urban areas—often located in hotter coastal regions—where declining fertility rates have led to slower growth or even population declines among children. Further research on regional fertility trends and migration patterns would help clarify whether these demographic shifts contribute to the observed decline in population influence on extreme heat exposures.

**Changes in Children's Heat Exposure Across Regions.** We present in Figure 4 Panels (a) and (b) regional-STAC statistics, which show the average shares of annual time at risk of heat stress for children in 1990 and 2020 across the four major economic regions of China. Figure 4 (c) shows the percentage-point change between 1990 and 2020 across these regions. Tables C.7 and C.8 in the online Appendix detail within-region provincial results.

Children in both the Central and Eastern regions experienced high levels of heat-stress exposures. For instance, in 1990, the average child in the Eastern and Central regions faced at-least-moderate-heat stress (UTCI $\geqslant 26\,^{\circ}$C) 23.6% and 23.4% of the time, and at-least-strong heat stress (UTCI $\geqslant 32\,^{\circ}$C) 8.4% and 9.3% of the time, respectively. The shares of time exposed to at-least-moderate or at-least-strong heat stress in these two regions remained high in 2020 as shown in Figure 4 Panel (b). The percentage-point increases in the shares of time at risk of heat exposure were notable across various UTCI thresholds in the Eastern region, with a 4.4 percentage-point increase at the 26 °C UTCI threshold and a 1.7 percentage-point increase at the 32 °C UTCI threshold. In contrast, for the Central region, the increases in the shares of time at risk remained at below one percentage point across UTCI thresholds (Figure 4 (c)). The comparison indicates that although Eastern- and Central-region children both have significant exposures to heat, those in the Eastern region have faced a heightened challenge in adapting to heat stress owing to the rapid increase in average exposure duration.

Compared to the Eastern and Central regions, the Northeastern region had relatively low average-child-heat exposure in 1990. However, the average child's share of annual time in the Northeastern region increased 19% for at-least-moderate-heat stress (UTCI $\geqslant 26\,^{\circ}$C) and 106% for at-least-strong-heat stress (UTCI $\geqslant 32\,^{\circ}$C). In 2020, the average Northeastern-region child

experienced 8.9% and 2.4% of her time under at-least-moderate (UTCI $\geqslant$ 26 °C) and at-least-strong (UTCI $\geqslant$ 32 °C) heat stress, respectively. While child-heat stress in the Northeastern region remained much lower than that in the Central and Eastern regions, the rapid increases indicate potential challenges for a population that is not accustomed to heat to protect children from emerging occurrences of heat stress.

Zooming in to the provincial level, in 2020, Hainan (Eastern), Guangdong (Eastern), Guangxi (Western), Jiangxi (Central), and Fujian (Eastern) were generally ranked as the top one-to-five provinces respectively in terms of the average shares of child time exposed to heat across UTCI thresholds. Specifically, in 2020, children in these provinces had on average 19.2%, 15.2%, 13.2%, 12.8%, and 11.8% shares of time exposed to at-least-strong-heat stress (UTCI $\geqslant$ 32 °C), which represented respective increases of 17%, 20%, 8%, 16%, and 54% in shares of time exposed compared to 1990. While Northeastern and Eastern provinces generally experienced substantial increases in heat exposure, provinces in the Central and Western regions experienced limited exposure increases or reductions. Tables C.7 and C.8 in the online Appendix detail within-region provincial results.

## 4 Discussion

As climatic change intensifies, the distributions of children's exposure to extreme heat are of critical concern for human development and public health (Connon and Dominelli 2022a; Park, Behrer, and Goodman 2021; Prentice et al. 2024; Zivin and Shrader 2016), but these distributions have received limited attention in past research. This study analyzed children's exposure to extreme heat in China across 30 years. Leveraging both geographical and temporal distributions of heat and of children, our study uncovered significant increases in children's exposures to moderate-or-stronger heat by an average of 238 hours from 1990 to 2020. The shares of children experiencing over 18 weeks per year of such heat stress more than doubled, indicating a growing vulnerability to heat exposure among children.

Our results highlighted the compound effect of rising temperatures and shifts in child-population-geographical distributions, particularly in a large nation like China with population and temperature distribution heterogeneities. The exposure to higher heat-stress levels, especially in the Eastern region, underscored the urgency for targeted interventions. This includes enhancing climate resilience and heat-stress mitigation strategies, especially in urban

areas where "heat island" effects may exacerbate high temperatures (Masson et al. 2020), as found in cities across China (Peng et al. 2018). Additionally, our findings underscored the importance of considering demographic changes in addition to climatic trends, as population shifts contributed significantly to the observed increase in heat exposure (Jones et al. 2015; Liu et al. 2017).

Conceptually, our approach to analyzing population-climatic exposure changes moved from the conventional metric of total person-time for measuring overall heat exposure burdens to a *double-dual-distributional* framework that considered both exposure intensity and exposure duration given changing population and climatic risk distributions. This approach enabled a comprehensive analysis of the shares of children experiencing 1) varying degrees of heat stress (exposure intensity) over 2) varying spans of time (exposure duration). It allowed for cross-time and cross-location comparisons. Moreover, this approach emphasized shifts in population-spatial distribution rather than changes in total population numbers, making it particularly valuable in identifying populations at risk of exposure in scenarios with substantial migration.

Our framework combined county-level census data with gridded-climatic data across time and space. We provided a framework for integrating population and climatic data for climatic and social scientists and policymakers interested in examining changing exposures of different populations to climatic (or other) hazards. While the availability of subnational and consistent global population data across long time spans is limited, subnational census data are publicly available for many countries across time and could be merged with publicly available global-temperature and other-climatic data to explore changes in population-based climatic exposures over time.

Our study has limitations. First, we examined ambient exposures rather than individually experienced exposures. Access to air conditioning or other adaptive resources can significantly influence the actual experience of heat stress (Xu, Sheffield, et al. 2014; Zivin and Shrader 2016). At an aggregate level, regions with similar ambient exposures but at different stages of economic development could also have varied levels of adaptability to the same heat stress (Braithwaite et al. 2024). Future research may benefit from examining the heterogeneities in adaptation to exposure measured in surveys. Second, while we use counties to provide a granular unit for jointly measuring child population and heat distributions in the Chinese and UTCI data settings (see Appendix Section B.2), finer spatial nuances of heat stress, particu-

larly in densely populated urban areas where microclimatic variations are significant (Wang et al. 2021; Zhou et al. 2015), were not investigated. Future research can build upon our study by integrating our frameworks with various definitions of heat exposure and using more fine-grained geographic units. Third, our analyses utilized variations over time in cross-sectional data. While this enables us to contribute important insights, it did not permit incorporating some important dynamics, such as the relations between climatic conditions and migration (Mueller, Gray, and Kosec 2014). Future work using longitudinal data could enrich the analyses by incorporating dynamics.

Despite these limitations, our study contributed new insights about the extent of heat-stress-exposure change for children between 1990 and 2020 in the country with the world's largest population of children in 1990. Importantly, we showed that changes in population distributions on the national level, though with variations among regions, were about as important as climatic changes. That the changing spatial distribution of children is a crucial component of changing-child-heat exposure risk is potentially relevant globally, given substantial shifts in recent decades in the distribution of the global child population across world regions (Hannum, Kim, and Wang 2024). The simple approach that we developed, moreover, permits new insights with minimal-data demands and therefore fruitfully could be easily applied to other countries and regions.

## References


Akresh, Richard. 2016. "Climate Change, Conflict, and Children." *The Future of Children* 26 (1): 51–71. https://www.jstor.org/stable/43755230.

All China Market Research Ltd. 2022. *2020 China County Population Census Data with GIS Maps.*

Arbuthnott, Katherine, Shakoor Hajat, Clare Heaviside, and Sotiris Vardoulakis. 2016. "Changes in Population Susceptibility to Heat and Cold Over Time: Assessing Adaptation to Climate Change." *Environmental Health* 15 (S1): S33. https://doi.org/10.1186/s12940-016-0102-7.

Baker, Rachel E., and Jesse Anttila-Hughes. 2020. "Characterizing the Contribution of High Temperatures to Child Undernourishment in Sub-Saharan Africa." *Scientific Reports* 10, no. 1 (November 2, 2020): 18796. https://doi.org/10.1038/s41598-020-74942-9.

Beijing Hua tong ren shi chang xin xi you xian ze ren gong si. 2005a. *1990 County Boundaries of China with Population Census Data, Part 1 & 2. [Shapefile].* https://geo.nyu.edu/catalog/nyu-2451-34775.

———. 2005b. *China Historical 2000 County Population Census Data.* https://geo.nyu.edu/catalog/harvard-ch-census2000.

Blazejczyk, Krzysztof, Gerd Jendritzky, Peter Broede, Dusan Fiala, George Havenith, Yoram Epstein, Agnes Psikuta, et al. 2013. "An Introduction to the Universal Thermal Climate Index (UTCI)" (January). https://doi.org/10.7163/GPol.2013.1'].

Braithwaite, Jeffrey, Elle Leask, Carolynn L. Smith, Genevieve Dammery, Kalissa Brooke-Cowden, Ann Carrigan, Ella McQuillan, et al. 2024. "Analysing Health System Capacity and Preparedness for Climate Change." *Nature Climate Change* 14, no. 5 (May): 536–546. https://doi.org/10.1038/s41558-024-01994-4.

Bröde, Peter, Dusan Fiala, Krzysztof Błażejczyk, Ingvar Holmér, Gerd Jendritzky, Bernhard Kampmann, Birger Tinz, et al. 2012. "Deriving the Operational Procedure for the Universal Thermal Climate Index (UTCI)." *International Journal of Biometeorology* 56, no. 3 (May 1, 2012): 481–494. https://doi.org/10.1007/s00484-011-0454-1.

Carleton, Tamma A., and Solomon M. Hsiang. 2016. "Social and Economic Impacts of Climate." *Science* 353, no. 6304 (September 9, 2016): aad9837. https://doi.org/10.1126/science.aad9837.

Chavez, Erik, Gordon Conway, Michael Ghil, and Marc Sadler. 2015. "An End-to-End Assessment of Extreme Weather Impacts on Food Security." *Nature Climate Change* 5, no. 11 (November): 997–1001. https://doi.org/10.1038/nclimate2747.

China Data Lab. 2020. *China County Map with 2000-2010 Population Census Data.* In collaboration with China Data Lab. https://doi.org/10.7910/DVN/VKGEBX.

Connon, Irena, and Lena Dominelli. 2022a. *Rapid Literature Review: Children and Heat Waves.* UNICEF Children's Climate Change Risk Index (CCRI). Data for Children Collaborative, September. https://www.dataforchildrencollaborative.com/outputs/rapidreview-heatwaves-tmha3.

———. 2022b. *Systematic Review of the Literature: Findings, Outcomes and Policy Recommendations.* UNICEF Children's Climate Change Risk Index (CCRI). Data for Children Collabortive and UNICEF, April. http://dspace.stir.ac.uk/handle/1893/34193.

Cooper, Matthew W., Molly E. Brown, Stefan Hochrainer-Stigler, Georg Pflug, Ian McCallum, Steffen Fritz, Julie Silva, et al. 2019. "Mapping the Effects of Drought on Child Stunting." *Proceedings of the National Academy of Sciences* 116, no. 35 (August 27, 2019): 17219–17224. https://doi.org/10.1073/pnas.1905228116.

Di Napoli, Claudia, Christopher Barnard, Christel Prudhomme, Hannah L. Cloke, and Florian Pappenberger. 2021. "ERA5-HEAT: A Global Gridded Historical Dataset of Human Thermal Comfort Indices from Climate Reanalysis." *Geoscience Data Journal* 8 (1): 2–10. https://doi.org/10.1002/gdj3.102.

Di Napoli, Claudia, Florian Pappenberger, and Hannah L. Cloke. 2018. "Assessing Heat-Related Health Risk in Europe Via the Universal Thermal Climate Index (UTCI)." *International Journal of Biometeorology* 62, no. 7 (July): 1155–1165. https://doi.org/10.1007/s00484-018-1518-2.

Ebi, Kristie L, Anthony Capon, Peter Berry, Carolyn Broderick, Richard De Dear, George Havenith, Yasushi Honda, et al. 2021. "Hot Weather and Heat Extremes: Health Risks." *The Lancet* 398, no. 10301 (August): 698–708. https://doi.org/10.1016/S0140-6736(21)01208-3.

Edwards, M. J., R. D. Saunders, and K. Shiota. 2003. "Effects of Heat on Embryos and Foetuses." *International Journal of Hyperthermia* 19, no. 3 (January 1, 2003): 295–324. https://doi.org/10.1080/0265673021000039628.

Gasparrini, Antonio, Yuming Guo, Masahiro Hashizume, Eric Lavigne, Antonella Zanobetti, Joel Schwartz, Aurelio Tobias, et al. 2015. "Mortality Risk Attributable to High and Low Ambient Temperature: A Multicountry Observational Study." *The Lancet* 386, no. 9991 (July 25, 2015): 369–375. https://doi.org/10.1016/S0140-6736(14)62114-0.

Grace, Kathryn, Frank Davenport, Heidi Hanson, Christopher Funk, and Shraddhanand Shukla. 2015. "Linking Climate Change and Health Outcomes: Examining the Relationship Between Temperature, Precipitation and Birth Weight in Africa." *Global Environmental Change* 35 (November 1, 2015): 125–137. https://doi.org/10.1016/j.gloenvcha.2015.06.010.

Grinsted, Aslak, John C. Moore, and Svetlana Jevrejeva. 2013. "Projected Atlantic Hurricane Surge Threat from Rising Temperatures." *Proceedings of the National Academy of Sciences* 110, no. 14 (April 2, 2013): 5369–5373. https://doi.org/10.1073/pnas.1209980110.

Guo, Yuming, Antonio Gasparrini, Ben Armstrong, Shanshan Li, Benjawan Tawatsupa, Aurelio Tobias, Eric Lavigne, et al. 2014. "Global Variation in the Effects of Ambient Temperature on Mortality: A Systematic Evaluation." *Epidemiology* 25, no. 6 (November): 781. https://doi.org/10.1097/EDE.0000000000000165.

Hannum, Emily, Jeonghyeok Kim, and Fan Wang. 2024. *From Population Growth to Demographic Scarcity: Emerging Challenges to Global Primary Education Provision in the Twenty-First Century.* Working Paper. May. https://jeonghyeok-kim.github.io/assets/GlobalChildrenTeachersSchools_HannumKimWang.pdf.

Harrington, Luke J., David J. Frame, Erich M. Fischer, Ed Hawkins, Manoj Joshi, and Chris D. Jones. 2016. "Poorest Countries Experience Earlier Anthropogenic Emergence of Daily Temperature Extremes." *Environmental Research Letters* 11, no. 5 (May): 055007. https://doi.org/10.1088/1748-9326/11/5/055007.

Helldén, Daniel, Camilla Andersson, Maria Nilsson, Kristie L. Ebi, Peter Friberg, and Tobias Alfvén. 2021. "Climate Change and Child Health: A Scoping Review and an Expanded Conceptual Framework." *The Lancet Planetary Health* 5, no. 3 (March 1, 2021): e164–e175. https://doi.org/10.1016/S2542-5196(20)30274-6.

Hsiang, Solomon M., Marshall Burke, and Edward Miguel. 2013. "Quantifying the Influence of Climate on Human Conflict." *Science* 341, no. 6151 (September 13, 2013): 1235367. https://doi.org/10.1126/science.1235367.

Hsu, Angel, Glenn Sheriff, Tirthankar Chakraborty, and Diego Manya. 2021. "Disproportionate Exposure to Urban Heat Island Intensity Across Major US Cities." *Nature Communications* 12, no. 1 (May 25, 2021): 2721. https://doi.org/10.1038/s41467-021-22799-5.

Jendritzky, Gerd, Richard de Dear, and George Havenith. 2012. "UTCI—Why Another Thermal Index?" *International Journal of Biometeorology* 56, no. 3 (May 1, 2012): 421–428. https://doi.org/10.1007/s00484-011-0513-7.

Jendritzky, Gerd, and Peter Höppe. 2017. "The UTCI and the ISB." *International Journal of Biometeorology* 61, no. 1 (September 1, 2017): 23–27. https://doi.org/10.1007/s00484-017-1390-5.

Jones, Bryan, Brian C. O'Neill, Larry McDaniel, Seth McGinnis, Linda O. Mearns, and Claudia Tebaldi. 2015. "Future Population Exposure to US Heat Extremes." *Nature Climate Change* 5, no. 7 (July): 652–655. https://doi.org/10.1038/nclimate2631.

Jones, Bryan, Claudia Tebaldi, Brian C. O'Neill, Keith Oleson, and Jing Gao. 2018. "Avoiding Population Exposure to Heat-Related Extremes: Demographic Change Vs Climate Change." *Climatic Change* 146, no. 3 (February 1, 2018): 423–437. https://doi.org/10.1007/s10584-017-2133-7.

Kovats, R. Sari, and Shakoor Hajat. 2008. "Heat Stress and Public Health: A Critical Review." *Annual Review of Public Health* 29 (Volume 29, 2008 2008): 41–55. https://doi.org/10.1146/annurev.publhealth.29.020907.090843.

Li, Long, and Yong Zha. 2020. "Population Exposure to Extreme Heat in China: Frequency, Intensity, Duration and Temporal Trends." *Sustainable Cities and Society* 60 (September): 102282. https://doi.org/10.1016/j.scs.2020.102282.

Li, Tiantian, Radley M. Horton, Daniel A. Bader, Maigeng Zhou, Xudong Liang, Jie Ban, Qinghua Sun, et al. 2016. "Aging Will Amplify the Heat-Related Mortality Risk Under a Changing Climate: Projection for the Elderly in Beijing, China." *Scientific Reports* 6, no. 1 (June 20, 2016): 28161. https://doi.org/10.1038/srep28161.

Liu, Xiaoying, Jere Behrman, Emily Hannum, Fan Wang, and Qingguo Zhao. 2022. "Same Environment, Stratified Impacts? Air Pollution, Extreme Temperatures, and Birth Weight in South China." *Social Science Research* 105 (July 1, 2022): 102691. https://doi.org/10.1016/j.ssresearch.2021.102691.

Liu, Zhao, Bruce Anderson, Kai Yan, Weihua Dong, Hua Liao, and Peijun Shi. 2017. "Global and Regional Changes in Exposure to Extreme Heat and the Relative Contributions of Climate and Population Change." *Scientific Reports* 7, no. 1 (March 7, 2017): 43909. https://doi.org/10.1038/srep43909.

Mahon, Michael B., Alexandra Sack, O. Alejandro Aleuy, Carly Barbera, Ethan Brown, Heather Buelow, David J. Civitello, et al. 2024. "A Meta-Analysis on Global Change Drivers and the Risk of Infectious Disease." *Nature* 629, no. 8013 (May): 830–836. https://doi.org/10.1038/s41586-024-07380-6.

Masson, Valéry, Aude Lemonsu, Julia Hidalgo, and James Voogt. 2020. "Urban Climates and Climate Change." *Annual Review of Environment and Resources* 45 (Volume 45, 2020 2020): 411–444. https://doi.org/10.1146/annurev-environ-012320-083623.

Mitchell, Bruce C., and Jayajit Chakraborty. 2015. "Landscapes of Thermal Inequity: Disproportionate Exposure to Urban Heat in the Three Largest US Cities." *Environmental Research Letters* 10, no. 11 (November): 115005. https://doi.org/10.1088/1748-9326/10/11/115005.

Mora, Camilo, Bénédicte Dousset, Iain R. Caldwell, Farrah E. Powell, Rollan C. Geronimo, Coral R. Bielecki, Chelsie W. W. Counsell, et al. 2017. "Global Risk of Deadly Heat." *Nature Climate Change* 7, no. 7 (July): 501–506. https://doi.org/10.1038/nclimate3322.

Mora, Camilo, Tristan McKenzie, Isabella M. Gaw, Jacqueline M. Dean, Hannah von Hammerstein, Tabatha A. Knudson, Renee O. Setter, et al. 2022. "Over Half of Known Human Pathogenic Diseases Can Be Aggravated by Climate Change." *Nature Climate Change* 12, no. 9 (September): 869–875. https://doi.org/10.1038/s41558-022-01426-1.

Mueller, V., C. Gray, and K. Kosec. 2014. "Heat Stress Increases Long-Term Human Migration in Rural Pakistan." *Nature Climate Change* 4, no. 3 (March): 182–185. https://doi.org/10.1038/nclimate2103.

Napoli, Claudia Di. 2020. *Thermal Comfort Indices Derived from ERA5 Reanalysis.* https://doi.org/10.24381/CDS.553B7518.

National Bureau of Statistics of China. 2011. *[Method of Dividing the East, West, Central and Northeast Regions].* Beijing: State Council of China, June 13, 2011. https://web.archive.org/web/20190323041213/http://www.stats.gov.cn/ztjc/zthd/sjtjr/dejtjkfr/tjkp/201106/t20110613_71947.htm.

———. 2021. *Main Data of the Seventh National Population Census.* Beijing: State Council of China, May 11, 2021. https://www.unicef.cn/en/media/24511/file/What%20the%202020%20Census%20Can%20Tell%20Us%20About%20Children%20in%20China%20Facts%20and%20Figures.pdf.

Onozuka, Daisuke, and Masahiro Hashizume. 2011. "The Influence of Temperature and Humidity on the Incidence of Hand, Foot, and Mouth Disease in Japan." *Science of The Total Environment* 410-411 (December 1, 2011): 119–125. https://doi.org/10.1016/j.scitotenv.2011.09.055.

Park, R. Jisung, A. Patrick Behrer, and Joshua Goodman. 2021. "Learning is Inhibited by Heat Exposure, Both Internationally and Within the United States." *Nature Human Behaviour* 5, no. 1 (January): 19–27. https://doi.org/10.1038/s41562-020-00959-9.

Pebesma, Edzer. 2018. "Simple Features for R: Standardized Support for Spatial Vector Data." *The R Journal* 10 (1): 439–446. https://doi.org/10.32614/RJ-2018-009.

Peng, Jian, Jing Ma, Qianyuan Liu, Yanxu Liu, Yi'na Hu, Yingru Li, and Yuemin Yue. 2018. "Spatial-Temporal Change of Land Surface Temperature Across 285 Cities in China: An Urban-Rural Contrast Perspective." *Science of The Total Environment* 635 (September): 487–497. https://doi.org/10.1016/j.scitotenv.2018.04.105.

Prentice, Caitlin M., Francis Vergunst, Kelton Minor, and Helen L. Berry. 2024. "Education Outcomes in the Era of Global Climate Change." *Nature Climate Change* 14, no. 3 (March): 214–224. https://doi.org/10.1038/s41558-024-01945-z.

Ren, Meng, Chunying Zhang, Jiangli Di, Huiqi Chen, Aiqun Huang, John S. Ji, Wannian Liang, et al. 2023. "Exploration of the Preterm Birth Risk-Related Heat Event Thresholds for Pregnant Women: A Population-Based Cohort Study in China." *The Lancet Regional Health - Western Pacific* 37 (August): 100785. https://doi.org/10.1016/j.lanwpc.2023.100785.

Romaszko, Jerzy, Ewa Dragańska, Rakesh Jalali, Iwona Cymes, and Katarzyna Glińska-Lewczuk. 2022. "Universal Climate Thermal Index as a Prognostic Tool in Medical Science in the Context of Climate Change: A Systematic Review." *Science of The Total Environment* 828 (July): 154492. https://doi.org/10.1016/j.scitotenv.2022.154492.

Sun, Xuerong, Fei Ge, Yi Fan, Shoupeng Zhu, and Quanliang Chen. 2022. "Will Population Exposure to Heat Extremes Intensify Over Southeast Asia in a Warmer World?" *Environmental Research Letters* 17, no. 4 (March): 044006. https://doi.org/10.1088/1748-9326/ac48b6.

Sun, Yida, Shupeng Zhu, Daoping Wang, Jianping Duan, Hui Lu, Hao Yin, Chang Tan, et al. 2024. "Global Supply Chains Amplify Economic Costs of Future Extreme Heat Risk." *Nature* 627, no. 8005 (March 28, 2024): 797–804. https://doi.org/10.1038/s41586-024-07147-z.

Sun, Ying, Xuebin Zhang, Francis W. Zwiers, Lianchun Song, Hui Wan, Ting Hu, Hong Yin, et al. 2014. "Rapid Increase in the Risk of Extreme Summer Heat in Eastern China." *Nature Climate Change* 4, no. 12 (December): 1082–1085. https://doi.org/10.1038/nclimate2410.

Tuholske, Cascade, Kelly Caylor, Chris Funk, Andrew Verdin, Stuart Sweeney, Kathryn Grace, Pete Peterson, et al. 2021. "Global Urban Population Exposure to Extreme Heat." *Proceed-*

*ings of the National Academy of Sciences* 118, no. 41 (October 12, 2021): e2024792118. https://doi.org/10.1073/pnas.2024792118.

UNICEF. 2021. "The Climate Crisis is a Child Rights Crisis," August 20, 2021. https://www.unicef.org/reports/climate-crisis-child-rights-crisis.

———. 2022. *The Coldest Year of the Rest of Their Lives: Protecting Children Form the Escalating Impacts of Heatwaves.* New York: UNICEF. https://www.unicef.org/media/129506/file/UNICEF-coldest-year-heatwaves-and-children-EN.pdf.

Walsh, Kevin J.E., John L. McBride, Philip J. Klotzbach, Sethurathinam Balachandran, Suzana J. Camargo, Greg Holland, Thomas R. Knutson, et al. 2016. "Tropical Cyclones and Climate Change." *WIREs Climate Change* 7, no. 1 (January): 65–89. https://doi.org/10.1002/wcc.371.

Wang, Jun, Yang Chen, Weilin Liao, Guanhao He, Simon F. B. Tett, Zhongwei Yan, Panmao Zhai, et al. 2021. "Anthropogenic Emissions and Urbanization Increase Risk of Compound Hot Extremes in Cities." *Nature Climate Change* 11, no. 12 (December): 1084–1089. https://doi.org/10.1038/s41558-021-01196-2.

Xi, Di, Linxin Liu, Min Zhang, Cunrui Huang, Katrin G. Burkart, Kristie Ebi, Yi Zeng, et al. 2024. "Risk Factors Associated with Heatwave Mortality in Chinese Adults Over 65 Years." *Nature Medicine* 30, no. 5 (May): 1489–1498. https://doi.org/10.1038/s41591-024-02880-4.

Xu, Zhiwei, Yang Liu, Zongwei Ma, Ghasem (Sam) Toloo, Wenbiao Hu, and Shilu Tong. 2014. "Assessment of the Temperature Effect on Childhood Diarrhea Using Satellite Imagery." *Scientific Reports* 4, no. 1 (June 23, 2014): 5389. https://doi.org/10.1038/srep05389.

Xu, Zhiwei, Perry E. Sheffield, Hong Su, Xiaoyu Wang, Yan Bi, and Shilu Tong. 2014. "The Impact of Heat Waves on Children's Health: A Systematic Review." *International Journal of Biometeorology* 58, no. 2 (March 1, 2014): 239–247. https://doi.org/10.1007/s00484-013-0655-x.

Zhou, Decheng, Shuqing Zhao, Liangxia Zhang, Ge Sun, and Yongqiang Liu. 2015. "The Footprint of Urban Heat Island Effect in China." *Scientific Reports* 5, no. 1 (June 10, 2015): 11160. https://doi.org/10.1038/srep11160.

Zivin, Joshua Graff, and Jeffrey Shrader. 2016. "Temperature Extremes, Health, and Human Capital." *The Future of Children* 26 (1): 31–50. https://doi.org/10.1353/foc.2016.0002.

Figure 1: Change in Share of Time for the Average Child at or above UTCI Thresholds for Children 1990-2020

(a) Changes between 1990 and 2020 in percentage points

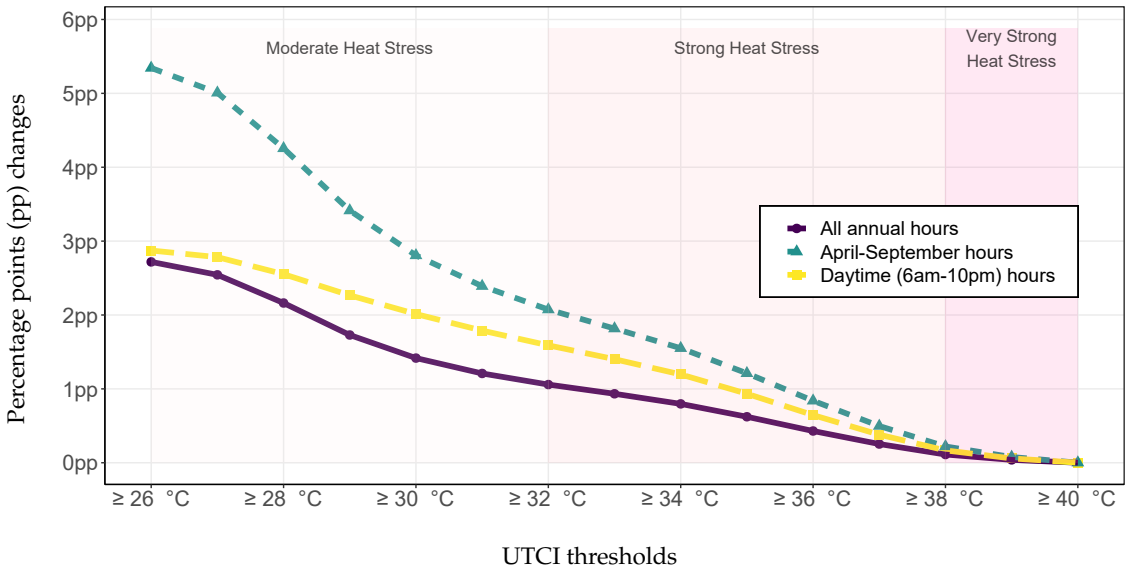


(b) Changes between 1990 and 2020 in percentage

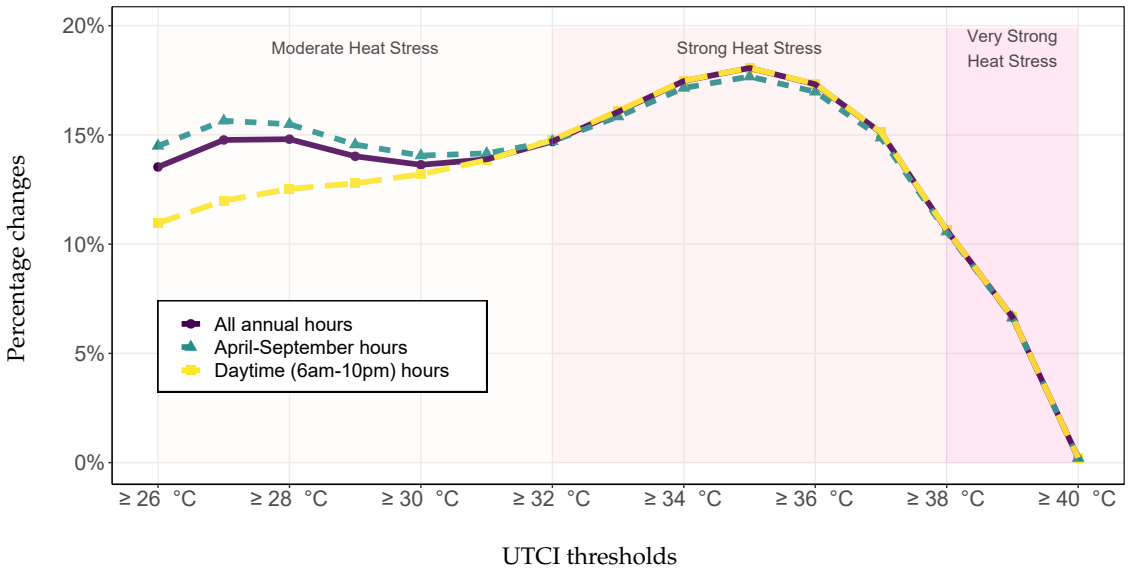


Notes: Panel (a) displays the percentage points (pp) change in the Share of Time for the Average Child at or above UTCI thresholds between 1990 and 2020, while Panel (b) displays the percentage changes in this share. The purple solid line represents results for all annual hours, the green short-dash line for the summer season (April to September), and the yellow long-dash line for daytime hours (6 am to 10 pm). Background colors indicate UTCI heat exposure categories. UTCI values above 26 to 32 degrees Celsius indicate moderate heat stress (light pink), from 32 to 38 degrees Celsius indicate strong heat stress (pink), and from 38 to 46 degrees Celsius indicate very strong heat stress (dark pink). Results above 40 degrees Celsius were not shown because very few children were exposed to such high levels of heat during the observed time periods in China. Tables C.1 and C.2 in the online Appendix tabulate results.

Figure 2: Share of Children Exposed to Heat Stress by Intensity and Duration

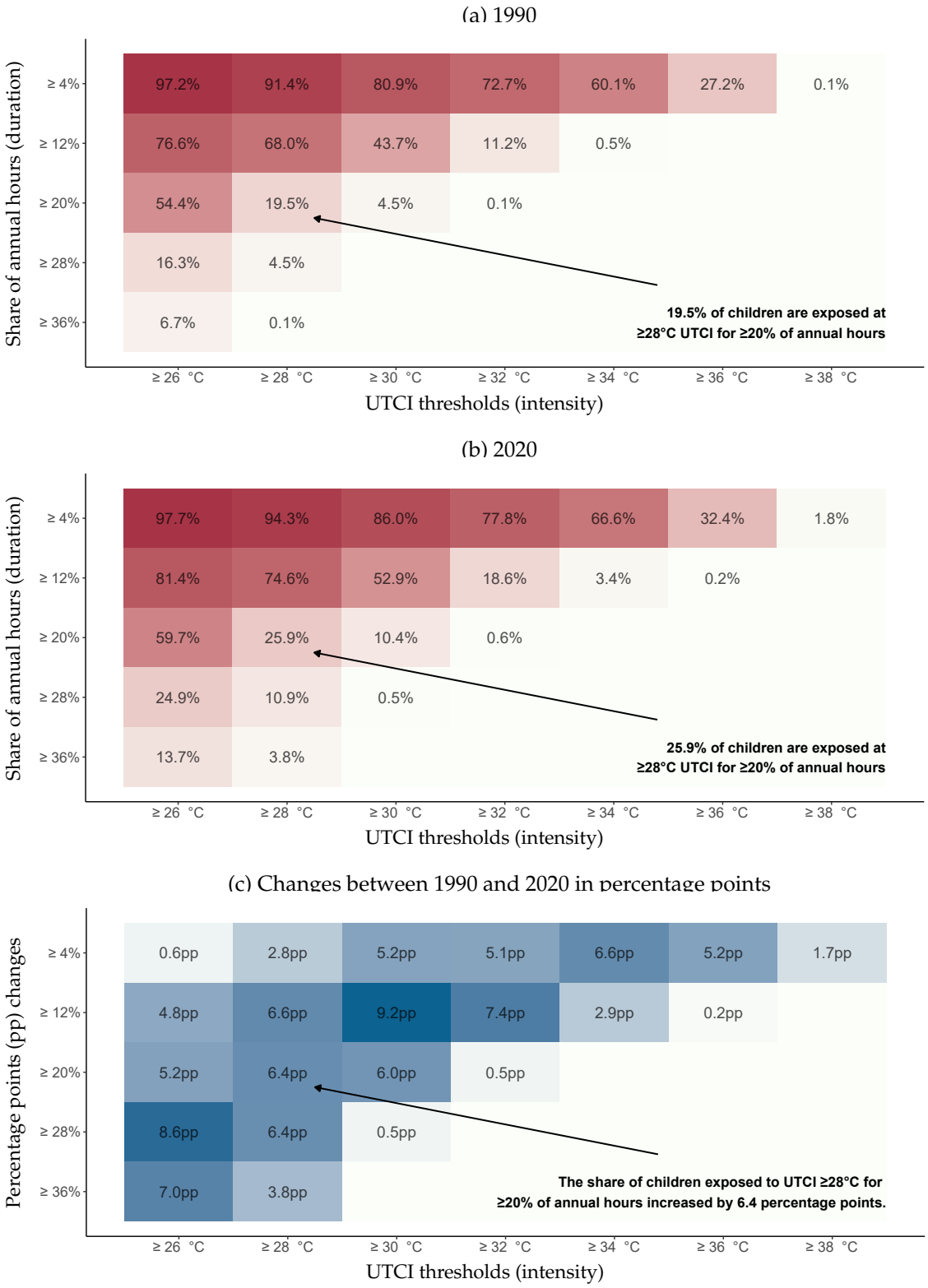


Notes: Panel (a) presents the share of children at risk of heat stress by duration and intensity in 1990. The duration is measured as the share of annual hours, whereas the intensity is measured as being at or above the UTCI threshold. Panel (b) presents the share of children at risk of heat stress by duration and intensity in 2020. Panel (c) presents the percentage points (pp) changes of children at risk of heat stress by duration and intensity between 1990 and 2020. Tables C.3 and C.4 in the online Appendix tabulate results.

Figure 3: Decomposed Change in Share of Time for the Average Child at Risk of Heat Stress

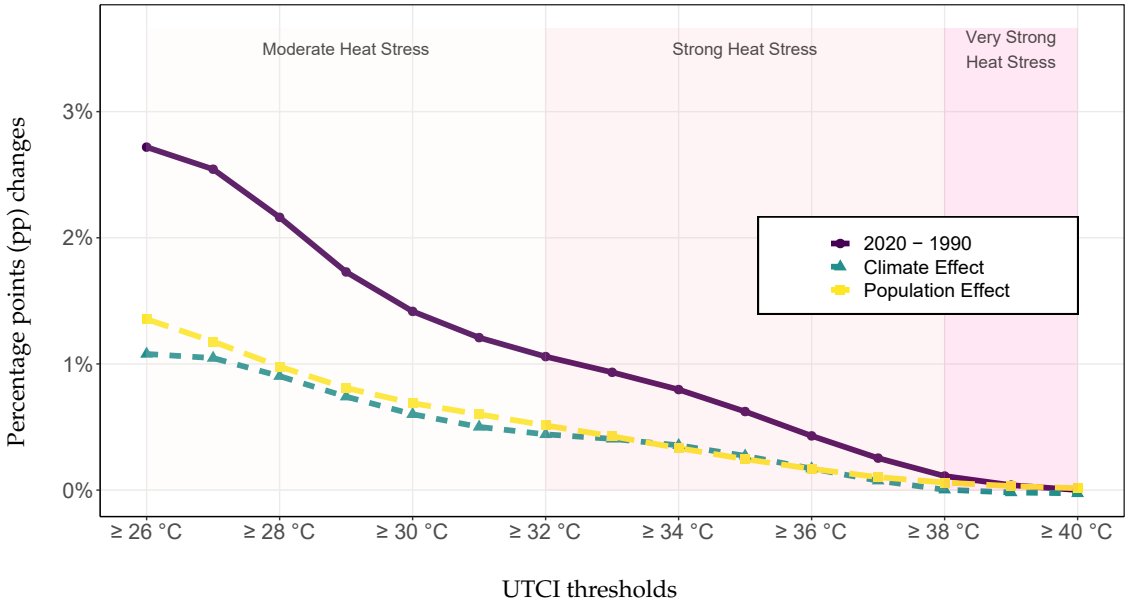


Notes: The purple solid line represents the percentage point difference in the share of time for the average child at risk of exposure to heat stress for children aged 0 to 14 between 1990 and 2020 (with 1990 as the baseline year). In the first counterfactual decomposition, we fix the children's population distribution in 1990 with the observed Universal Thermal Climate Index (UTCI) in 2020. The green short-dash line, or the climate effect, represents the percentage difference between the first counterfactual decomposition results and the baseline (using 1990 children's population distribution with 1990 UTCI). In the second counterfactual decomposition, we fix the UTCI at the 1990 level and use the children's population distribution in 2020. The yellow long-dash line, or the population effect, represents the percentage difference between the second counterfactual decomposition results and the baseline. Tables C.5 and C.6 in the online Appendix tabulate the results.

Figure 4: Regional Share of Time for the Average Child at Risk of Heat Stress

(a) 1990

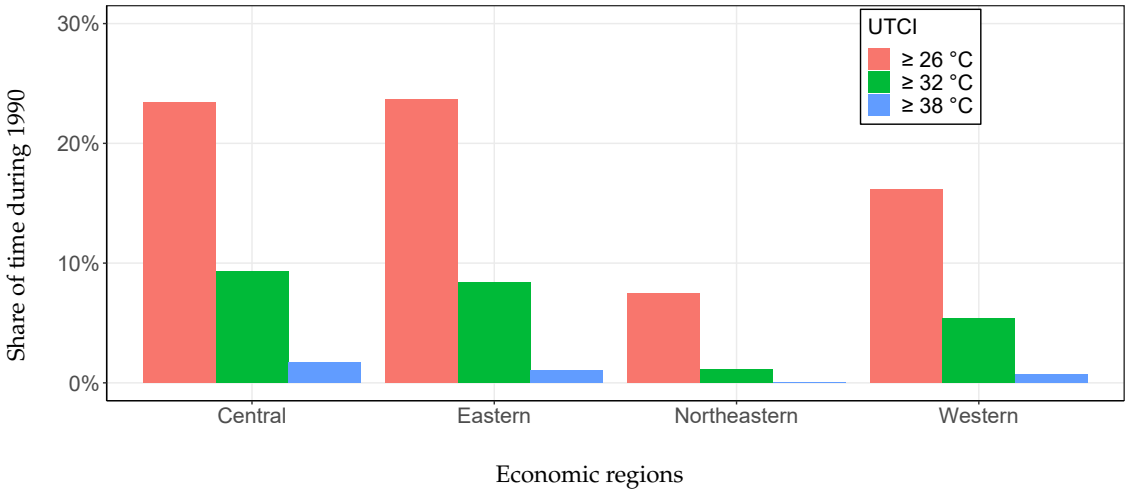


(b) 2020

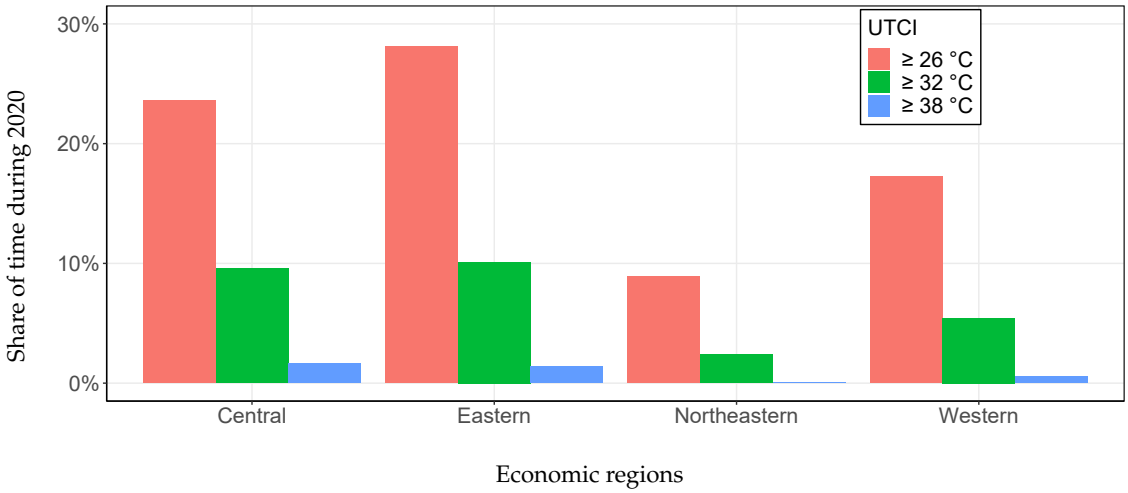


(c) Changes between 1990 and 2020 in percentage points

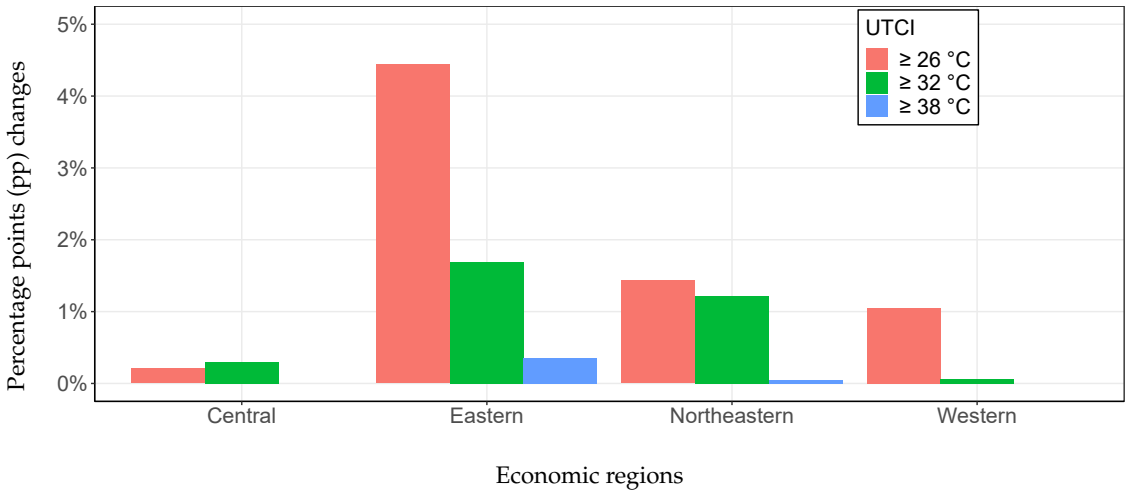


Notes: The y-axis depicts the percentage point difference from 2020 and 1990 heat exposure for children ages 0-14. We display these differences across the four economic regions of China and across different thresholds of heat exposure (moderate, strong, and very strong). Tables C.7 and C.8 in the online Appendix tabulate results.

Supplemental Information

# Rising Temperatures, Rising Risks: Changes in Chinese Children's Ambient Heat Exposure between 1990 and 2020

Kai Feng, Marco M. Laghi, Jere R. Behrman, Emily Hannum, and Fan Wang

## A Method

**Location- and Period-specific Heat Exposure** We now formalize our heat exposure analysis framework across time and space. Specifically, let $c_l(t)$ be the UTCI temperature experienced by an individual at a moment in time $t$ at a location $l$. Between period $t$ and $t+\tau$, the share of time that individuals at location $l$ experience temperature $c_l(t)$ over threshold $c^*$ is, $s_l(c^*, t, \tau)$:

$$s_l(c^*, t, \tau) = \frac{1}{\tau} \int_t^{t+\tau} \mathbf{1}\{c_l(t) > c^*\} \, dt \, . \tag{1}$$

Depending on the analysis, our definition of time period includes all time during the day, all day time hours (6 am to 10 pm), or all hours within different seasons (e.g., April–September, October–March). Additionally, let $P_{t \leqslant t < t+\tau}(l|m)$ be the share of population for socio-demographic group $m$ in a location $l$, among $L$ locations in total between time $t$ and $t+\tau$. Total population shares across locations sum up to 1: $\sum_{l=1}^{L} P_{t \leqslant t < t+\tau}(l|m) = 1$.

**Average Share of Time of Heat Exposure** We compute two key sets of statistics. First, we compute $\mathcal{S}_m(c^*, t, \tau)$, which measures, during a particular interval of time, the average share of time individuals of socio-demographic group $m$ are exposed to UTCI temperatures over threshold $c^*$:

$$\mathcal{S}_m(c^*, t, \tau) = \sum_{l=1}^{L} P_{t \leqslant t < t+\tau}(l|m) \cdot s_l(c^*, t, \tau) \, . \tag{2}$$

$\mathcal{S}_m(c^*, t, \tau)$ is the *Share of Time for the Average Child* (STAC) statistic, which measures, for the average child, the share of time exposed to ambient extreme UTCI temperature during a particular time-frame across heat stress thresholds.

Since $\mathcal{S}_m(c^*, t, \tau)$ is a statistics for share of time, it varies between 0 and 1. In particular, $\lim_{c^* \to \infty} \mathcal{S}_m(c^*, t, \tau) = 0$ and $\lim_{c^* \to -\infty} \mathcal{S}_m(c^*, t, \tau) = 1$. A key aggregate statistic for how

heat exposure shifts between period $t'$ and $t$ is the following difference:

$$\Delta \mathcal{S}_{m,t',t}(c^*, \tau) = \mathcal{S}_m\left(c^*, t', \tau\right) - \mathcal{S}_m(c^*, t, \tau). \tag{3}$$

$\Delta \mathcal{S}_{m,t',t}(c^*, \tau)$ is the population-weighted average increase in the share of time exposed to the potential key heat stress threshold $c^*$ between time $t$ and $t'$ for population group $m$. $\Delta \mathcal{S}_{m,t',t}(c^*, \tau)$ shifts due to both shifts in the population distribution as well as the distribution of UTCI temperature between $t$ and $t'$, thus taking into account both population and meteorological changes across time and space.

**Share of Children by Duration and Intensity of Heat Exposure** Second, we compute the share of individuals at risk, based on a joint consideration of the relevant heat stress threshold that might be considered risky for human development, and the share of time exposed to such heat that would put individuals at risk of non-transitory impacts.

We consider these two joint dimensions of risks in computing population exposure statistics. Specifically, let $s^*(\tau)$ be a particular share-of-time threshold within span of time $\tau$ above a specific heat stress threshold. We define the $m$-, $c^*$-, and $s^*$-specific at-risk measure $\mathcal{R}_m(c^*, s^*, t, \tau)$ between time $t$ and $t + \tau$ as:

$$\mathcal{R}_m(c^*, s^*, t, \tau) = \sum_{l=1}^{L} P_{t \leqslant t < t+\tau}(l|m) \cdot \mathbf{1}\{s_l(c^*, t, \tau) > s^*(\tau)\}. \tag{4}$$

$\mathcal{R}_m(c^*, s^*, t, \tau)$ is the *Share Exposed by Intensity and Duration Thresholds* (SEIDT) statistic, which measures the share of children exposed to extreme heat by differing UTCI temperature (intensity) and time (duration) thresholds.

By construction, $\mathcal{R}_m(c^*, s^* = 0, t, \tau) \leqslant 1$ and $\mathcal{R}_m(c^*, s^* = 1, t, \tau) = 0$. Additionally, the share of individuals experiencing greater than $s^*$ share of time over $c^*$ threshold converges to 0 as $c^*$ increases: $\lim_{c^* \to \infty} \mathcal{R}_m(c^*, s^*, t, \tau) = 0$.

For the socio-demographic group indexed by $m$, given heat stress threshold $c^*$ and share of time threshold $s^*$, the percentage increase over time in the share of individuals from this group at risk of excess heat exposure is:

$$\Delta \mathcal{R}_{m,t',t}(c^*, s^*, \tau) = \mathcal{R}_m\left(c^*, s^*, t', \tau\right) - \mathcal{R}_m(c^*, s^*, t, \tau). \tag{5}$$

One important aspect of our framework is that computing $\mathcal{R}_m\left(c^*, s^*, t, \tau\right)$ and $\Delta\mathcal{R}_{m,t',t}\left(c^*, s^*, \tau\right)$ do not require the use of harmonized geographic data overtime. This is often a constraint in the analysis of UTCI temperature changes over time, due to shifting administrative boundaries, especially across large spans of time. In our framework, we consider all $l \in \{1, \ldots, L\}$ locations within a region, and generate time-specific population-UTCI temperature cumulative distribution functions by sorting locations along the gradient of heat exposures and summing up the share of population for socio-demographic group $m$ along ascending levels of heat exposures. While our distributions are discretized by location-level administrative units, when there are large number of locations with dispersed population, the population-UTCI temperature distributions tend to be approximately smooth. Cross-time comparisons, especially at higher levels of regional aggregation, are based on these approximately smooth distributions over time. Hence moments and percentiles of these population-UTCI temperature distributions are robust to shifts in sub-region location boundaries.

**Framework and Empirical Results** In our empirical application, $t$ is 1990 and, $t'$ is 2020, $\tau$ is one calendar year, and $m$ is children between ages 0 and 14. Additionally, we approximate continuous time with hourly measurements. As an example, $\Delta\mathcal{R}_{\text{children,2020,1990}}$ with $c^* = 28$ and $s^* = 0.1$ provides the change in the percentage points of children exposed to UTCI temperature over 28 degrees for greater than 10 percent of their time during a year.

Results for $\Delta\mathcal{S}_{m=\text{ages 0 to 15},t'=\text{year 2020},t=\text{year 1990}}\left(c^*, \tau = 1 \text{ year}\right)$ are summarized in Figure 1 and Tables C.1 and C.2. These capture changes in the average share of time children are exposed to UTCI temperature over a range of heat thresholds—$23°C \leqslant c^* \leqslant 40°C$—considering all hours, day time hours, or hours during hotter and colder seasons.

Results for $\Delta\mathcal{R}_{m=\text{ages 0 to 15},t'=\text{year 2020},t=\text{year 1990}}\left(c^*, s^*, \tau = 1 \text{ year}\right)$ are summarized in Figure 2 and Tables C.3 and C.4. These capture changes in the share of children experiencing ambient heat exposure for over a range of $c^*$ heat *intensity* thresholds—$23°C \leqslant c^* \leqslant 40°C$—and $s^*$ heat exposure *duration* thresholds—4% of year $\leqslant s^* \leqslant$ 36% of year.

Additionally, Figure 3 and Tables C.5 and C.6 summarize decompositional results that compute changes in the average share of time of child exposure, but combining 1990 population distribution with 2020 heat exposure distribution, and also 1990 heat exposure distribution with 2020 population distribution. Finally, Figure 4 and Tables C.7 and C.8 provide regional results on the changes in the average share of time of child exposure.

# B Data

## B.1 Population and Heat Data Sources

**ERA5 Data Details** To measure heat, we used the fifth generation of the European Centre for Medium-Range Weather Forecasts (ECMWF) atmospheric reanalyses of the global climate: the ERA5-HEAT dataset (Di Napoli et al. 2021; Napoli 2020). Covering the period from 1940 to the present, ERA5-HEAT comprises hourly gridded maps of the Universal Thermal Climate Index (UTCI) at 0.25° × 0.25° spatial resolution. The dataset is publicly accessible through the Copernicus Climate Change Service's Climate Data Store (CDS). The UTCI is a widely used index to assess the human-perceived thermal stress based on atmospheric conditions, integrating atmospheric parameters like temperature, humidity, wind speed, and solar radiation. UTCI is expressed in degrees Celsius (°C), and it provides a measure of how cold or hot people might feel under prevailing environmental conditions (Blazejczyk et al. 2013; Bröde et al. 2012; Jendritzky, Dear, and Havenith 2012; Jendritzky and Höppe 2017). When UTCI is between 26 °C and 32 °C, it indicates moderate-heat stress on the human body, signifying warm conditions where individuals may start to feel uncomfortable, especially if engaging in physical activity. As the UTCI value increases, the level of thermal stress on the human body intensifies. UTCI values between 32 °C and 38 °C indicate strong-heat stress, whereas UTCI values between 38 °C and 46 °C indicate very-strong-heat stress (Bröde et al. 2012). We utilized these UTCI stress categories in this study.

**Census Population Data Details** For population data, we utilized Chinese-census data for the years 1990 and 2020 (All China Market Research Ltd 2022; Beijing Hua tong ren shi chang xin xi you xian ze ren gong si 2005a, 2005b; China Data Lab 2020). County-level child population data and county-level administrative boundary files were extracted and used to construct ages 0–14 populations by county. For regional analysis, we considered the child population and UTCI distributions within each one of the four recognized economic regions of China (National Bureau of Statistics of China 2011).

We use information from 2,369 geographical units at the county level nested in 31 provincial administrative units from the Tabulation on 1990 China Population Census by County. We start with the 1990 Chinese Census as it is the first to offer county-level population counts for individuals between ages 0 to 14. We only include mainland China and do not include special

administrative regions. Within each county, we calculate the sum of ages 0 to 14 child population regardless of gender. In 1990, the total number of children across all counties included for analysis was 312,995,886.

We use information from 2,853 geographical units at the county level nested in 31 provincial administrative units from the Tabulation on 2020 China Population Census by County. We only include mainland China and do not include special administrative regions. We again calculate the population counts for children between ages 0 to 14, regardless of gender, in our analysis. In 2020, the total number of children across all counties included for analysis was 249,260,992.

### B.2 Child Population-weighted Heat Distribution

Depending on our analysis, we consider all county-level administrative units in China, in a region, or in a province, and generate year-specific child-population-weighted (for children ages 0–14) UTCI cumulative distribution by sorting counties along ascending levels of heat exposure and summing up the share of child population county-by-county along the ascending levels of heat exposure.

In this section, we show the population- and spatial-granularity of our county-based analysis and find that counties provide a granular unit for child population and heat measurement in the Chinese and UTCI data setting. We use population data from 2369 (in 1990) and 2853 (in 2020) county-level administrative units and heat data from 15,432 gridded UTCI data points that cover mainland China. We find that child population is widely dispersed across counties (see Table B.1), and this leads to child-population-weighted heat distributions that are approximately smooth and do not contain large discretized "steps." Additionally, we find that most Chinese counties, with the exception of large western counties with small child population levels, have limited geographical expanse and hence limited number of within-county UTCI measurements (see Table B.2). This means that county mean heat levels summarize well the UTCI-based ambient heat exposure measurements within counties.

It is important to note that the geography of county-level administrative boundaries shifted significantly between 1990 and 2020. But our child-population based analysis does not compare each county-level unit over time, instead, we compare the year-specific national and regional fine-grained child-population-weighted heat distributions using cross-county information.

**The Distribution of Children Across Counties** In Table B.1, we order county-level administrative units by their child population counts, and construct county-level national and regional child-population distributions. Panel A shows national distributions while Panels B through E show results from regional distributions. Overall, the results show that county-level administrative units provide a granular unit for constructing child-population-weighted statistics in the Chinese setting.

Nationally, we find that child population is widely dispersed across counties. The median Chinese county-level administrative unit accounts for 0.057% (186 thousand children) of the national child population in 1990 and 0.051% (128 thousand children) in 2020, while the county at the 99th percentile of child-population distribution accounts for 0.382% (1.240 million children) in 1990 and 0.276% (690 thousand children) of the national child population in 2020.

Regionally, child population is also widely dispersed across counties, with some variations over time. We see that in 1990, the median county in Western China accounts for 0.042% (137 thousand children) of the national child population, about four fifth of the median share in Northeastern China (0.051%, 165 thousand children) and two third of the median share in Eastern (0.063%, 206 thousand children) and Central (0.066%, 216 thousand children) China. Due to an increase in the number of counties per region and an overall decrease in total child population, in 2020, the share and number of children in Chinese counties decreased compared to 1990, across regions. Specifically, in 2020, the median county in Western, Northeastern, Eastern, and Central China accounts for 0.040% (99 thousand children), 0.021% (52 thousand children), 0.060% (151 thousand children), and 0.057% (143 thousand children) percent of the national child population in China. The largest counties in terms of child population appear in Eastern China and also only account for a small fraction of the national population: In 1990 and 2020, the county at the 99th percentile of Eastern China's child population distribution accounts for 0.448% (1.453 million) and 0.551% (1.376 million) of the national child population, respectively.

**The Distribution of Grid Points Across Counties** In Table B.2, we present the distribution of UTCI grid points across counties and the distribution of children across counties in 1990 and 2020. We first show the number of grid points in column one, followed by the number of counties across 1990 and 2020 matched to different numbers of overlapping grid points, with the fourth and fifth columns depicting the percentage of children within those counties. The

remaining columns depict the row-cumulative percentage of children.

We find that most Chinese counties have limited geographic expanse, and this allows the matching of granular child population information to granular gridded heat measurements. More specifically, in 1990, 41% of counties (970 counties) intersect with two or fewer UTCI spatial grid points, and these counties account for 41% of the total child population. Additionally, 77% of counties (1,826 counties) intersect with five or fewer UTCI spatial grid points, and these counties account for 83% of the total child population. In 2020, 51% of counties (1,465 counties) intersect with two or fewer UTCI spatial grid points, and these counties account for 55% of the total child population. Additionally, 81% of counties (2,323 counties) intersect with five or fewer UTCI spatial grid points, and these counties account for 89% of the total child population. Overall, in both 1990 and 2020, more than 95% of children reside in counties that are associated with ten or fewer grid points. Using information for the city of Shanghai and Henan Province, Figure B.1 and Figure B.2 provide illustrative examples of the overlap between county-level administrative boundaries and UTCI grid points, respectively.

Some county-level administrative units, in particular from Western China, are geographically expansive, and pose a challenge to our county-based analysis. Specifically, 39 counties in 1990 and 41 counties in 1990 overlapped with between 51 and 330 gridded UTCI points (see Table B.2). Figure B.3 illustrates this with the example of Western China's Qinghai province, which has several geographically large county-level administrative areas toward the western side of the province. Heat levels can vary substantially across these gridded points and we do not have disaggregated child population data within these counties. However, the share of child population in these counties is only about 0.1% of the national population, and aggregation-errors in these areas do not measurably impact national and regional child-population weighted distributional statistics.

### B.3 Merging Climatic and Population Data

All project data processing, integration, and analysis code are shared at our project repository: https://github.com/ClimateInequality/PrjCEC. In this section, we summarize key aspects of how we integrate climatic and population data to enable the analysis of changes over time in heat burden facing children. Specifically, code for generating computing population-weighted exposure statistics are included in the R folder, and integrated population-climate data outputs for each analysis included in the paper are stored in the data-res folder.

In this section, we provide additional technical details on the ERA5-Heat and child population data sources and the data merging process.

**ERA5-HEAT Data Input Specification** To capture the entire mainland China area, we employ China's far-east (135°E), far-west (53°E), far-south (4°N), and far-north (54°N) points as spatial references in our API request to extract a rectangle area that contains gridded data covering latitude and longitude coordinates that encompass mainland China from the ERA5-HEAT data. We specify all months, dates, and hours in calendar years 1990 and 2020 in our API request. After downloading coordinate-specific hourly UTCI from all dates, we consolidate them into data files by year. For example, in the 2020 data file, corresponding to each coordinate in the gridded map (data rows), we include UTCI values for all hours between January 1, 2020 to December 31, 2020 (data columns).

**Population Data Input Specification** We obtain county-level demographic data from census tabulations. In each census file, there is one unique identification number for each county-level administrative unit. Each county includes demographic data by age group and gender for the corresponding census year. The county-level shapefile for each census year provides geometries defining the boundaries of each county. The geometry information for each county—summarized by county-specific sets of polygon-bounding vertices in longitude and latitude units—is important for linking the population data with the gridded UTCI data.

The final population input consists of a data matrix. In this matrix, the first column identifies a distinct county-level administrative unit ID, while other columns store the proportion of the population between ages 0 to 14 in each county relative to the total population between ages 0 to 14 during one census year. While our focus is on children between ages 0 to 14, our approach has the flexibility to be extended to any demographic group as needed.

**Specifying Key Files** There are three key files necessary for linking population data input and UTCI input: (1) key file that links the coordinates to counties. (2) key file that links county to province and regions. (3) key file that links population input column variables to the original labels (e.g., age groups and gender), and grouping variables for aggregation purposes (i.e., age groups 0-14, 15-64, 65+).

*Coordinates to counties.* We use spatial join from the "sf" package in R (Pebesma 2018) to identify grid point coordinates from UTCI data that fall within each county boundary. When

only one grid point falls within a county boundary, its attribute value is used to represent the county. When a county zone contains no grid points, the UTCI from the nearest grid point to the county centroid is assigned to the county (see Figure B.1). 127 counties in 1990 and 393 counties in 2020 do not contain grid points and require assignment. When multiple grid points fall within the county, the average of their attribute values (i.e., UTCI) is calculated to represent the county (see Figures B.2 and B.3). The final key file includes a list of coordinates, with each coordinate matched with the corresponding county-level administrative code in China. The county code provides linkages to the county-level population census, while the coordinates provides linkages to the gridded ERA5-HEAT data.

*County to province/region.* Each county code can be linked back to the province and economic regions that the county belong to. In addition to province, we can easily aggregate the county to other higher level units.

*Population input columns to labels.* This key file provides label names to the population input columns.

Figure B.1: Chinese Counties and UTCI Grids, Shanghai

(a) 1990 districts/counties

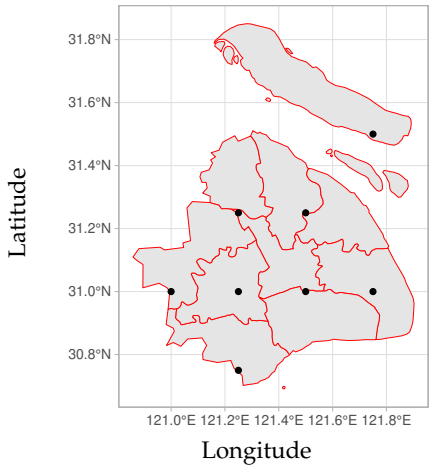


(b) 2020 districts/counties

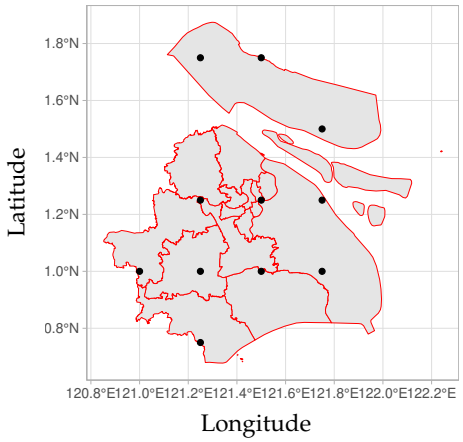


Notes: We superimpose UTCI grid points (0.25° × 0.25° longitude–latitude grid) over the 1990 and 2020 district/county-level administrative boundaries (red boundary lines) from Shanghai, China. We show grid points (shown as black dots) that fall within the boundary of at least one district/county-level administrative unit. We associate county-level child population data with the average hourly temperature of grid points that fall within the boundaries of the county-level administrative unit. For Shanghai counties that do not overlap with any grid points, we associate children in the county with the hourly UTCI of the spatial grid point closest to the county's centroid.

Figure B.2: Chinese Counties and UTCI Grids, Henan

(a) 1990 counties

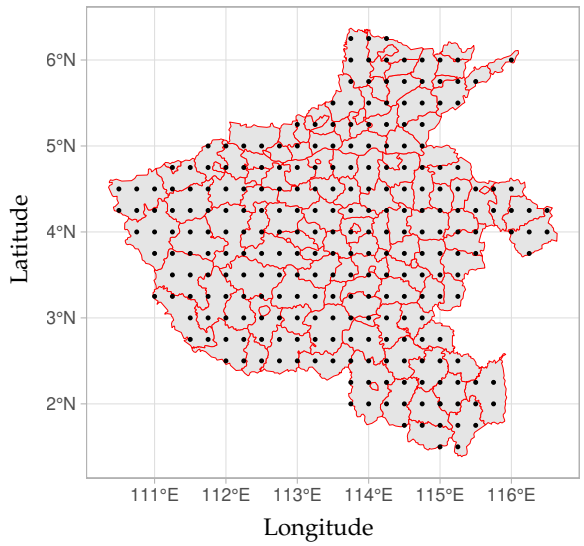


(b) 2020 counties

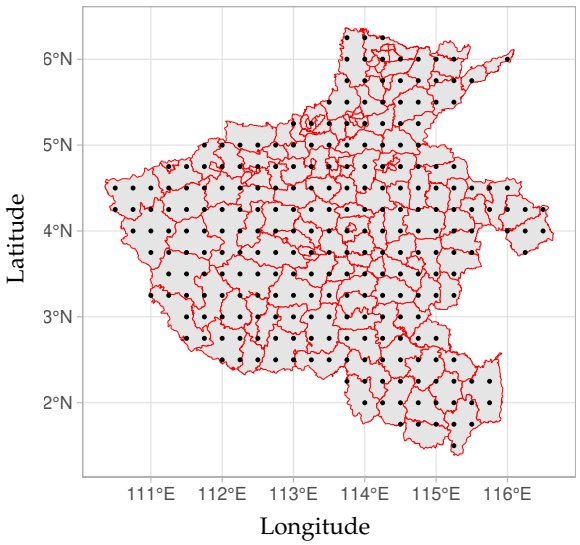


Notes: We superimpose UTCI grid points ($0.25° \times 0.25°$ longitude–latitude grid) over the 1990 and 2020 county-level administrative boundaries (red boundary lines) from Henan, China. We show grid points (shown as black dots) that fall within the boundary of at least one county-level administrative unit. We associate county-level child population data with the average hourly temperature of grid points that fall within the boundaries of the county-level administrative unit.

Figure B.3: Chinese Counties and UTCI Grids, Qinghai

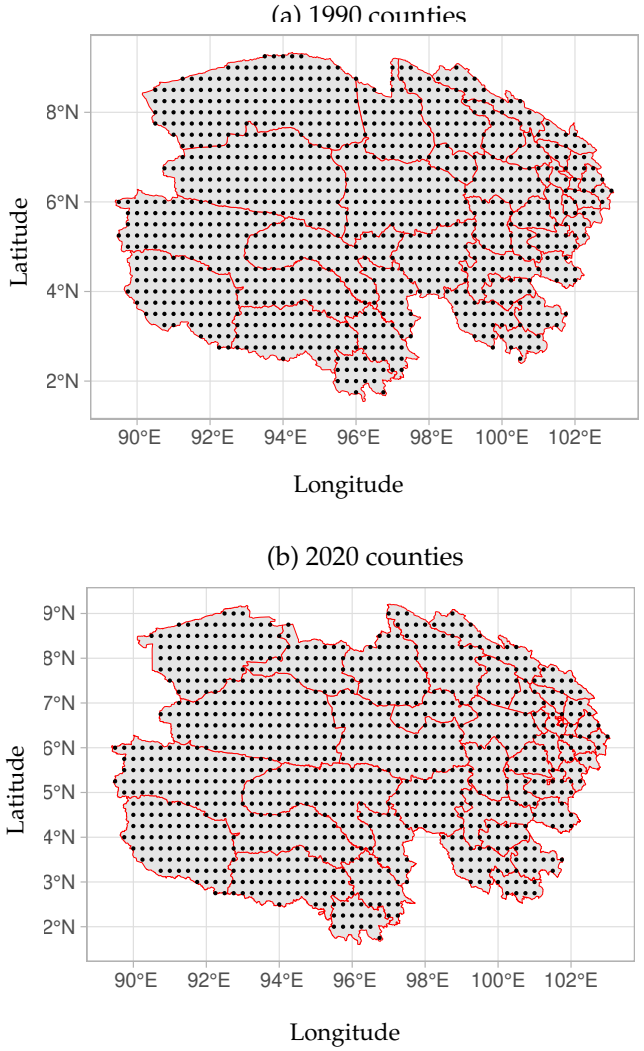


Notes: We superimpose UTCI grid points (0.25° × 0.25° longitude–latitude grid) over the 1990 and 2020 county-level administrative boundaries (red boundary lines) from Qinghai, China. We show grid points (shown as black dots) that fall within the boundary of at least one county-level administrative unit. We associate county-level child population data with the average hourly temperature of grid points that fall within the boundaries of the county-level administrative unit.

Table B.1: The Distribution of Chinese Children (ages 0-14) Across Counties in 1990 and 2020

| | | Percentiles | | | | | | |
|---|---|---|---|---|---|---|---|---|
| Statistics | Year | 1 | 10 | 25 | 50 | 75 | 90 | 99 |
| **Panel A: National** | | | | | | | | |
| Number | 1990 | 27.5K | 79.3K | 117.0K | 185.7K | 291.0K | 405.5K | 1240.1K |
| Percent | 1990 | 0.008% | 0.024% | 0.036% | 0.057% | 0.09% | 0.125% | 0.382% |
| Number | 2020 | 15.5K | 47.9K | 77.4K | 128.3K | 201.7K | 296.0K | 689.6K |
| Percent | 2020 | 0.006% | 0.019% | 0.031% | 0.051% | 0.081% | 0.118% | 0.276% |
| **Panel B: Central region** | | | | | | | | |
| Number | 1990 | 39.6K | 89.9K | 140.9K | 215.7K | 312.4K | 404.9K | 540.0K |
| Percent | 1990 | 0.012% | 0.028% | 0.043% | 0.066% | 0.096% | 0.125% | 0.166% |
| Number | 2020 | 20.3K | 54.7K | 86.7K | 142.7K | 209.3K | 270.6K | 374.3K |
| Percent | 2020 | 0.008% | 0.022% | 0.035% | 0.057% | 0.084% | 0.108% | 0.15% |
| **Panel C: Eastern region** | | | | | | | | |
| Number | 1990 | 52.2K | 94.3K | 138.1K | 206.0K | 320.9K | 486.7K | 1453.2K |
| Percent | 1990 | 0.016% | 0.029% | 0.043% | 0.063% | 0.099% | 0.15% | 0.448% |
| Number | 2020 | 33.3K | 67.8K | 97.9K | 150.8K | 239.1K | 378.8K | 1376.4K |
| Percent | 2020 | 0.013% | 0.027% | 0.039% | 0.06% | 0.096% | 0.152% | 0.551% |
| **Panel D: Northeastern region** | | | | | | | | |
| Number | 1990 | 25.2K | 83.9K | 116.8K | 165.4K | 249.8K | 332.4K | 984.1K |
| Percent | 1990 | 0.008% | 0.026% | 0.036% | 0.051% | 0.077% | 0.102% | 0.303% |
| Number | 2020 | 6.0K | 21.5K | 33.4K | 51.5K | 76.4K | 116.9K | 233.0K |
| Percent | 2020 | 0.002% | 0.009% | 0.013% | 0.021% | 0.031% | 0.047% | 0.093% |
| **Panel E: Western region** | | | | | | | | |
| Number | 1990 | 14.6K | 54.9K | 90.1K | 137.3K | 238.4K | 350.5K | 563.6K |
| Percent | 1990 | 0.004% | 0.017% | 0.028% | 0.042% | 0.073% | 0.108% | 0.174% |
| Number | 2020 | 10.6K | 37.1K | 62.4K | 99.4K | 164.9K | 235.4K | 405.0K |
| Percent | 2020 | 0.004% | 0.015% | 0.025% | 0.04% | 0.066% | 0.094% | 0.162% |

*Note:* Drawing on the 1990 and 2020 Chinese census, we present key percentiles of county-level distributions of the child population (ages 0–14) in China in 1990 and 2020. In the rows where the statistics are labelled "Number", we show the number of children in units of thousands of children. In the rows where the statistics are labelled "Percent", we show the percent of children in a county as a share of the overall child population (ages 0–14) in the country. We present national and regional results. The statistics show, for example, that in 1990, the median county in China had 185.7 thousand children, which is equivalent to 0.057% of the overall child population (ages 0–14) in the country. Across all panels representing regional and national contexts, any one county provides a small amount of the child population data, for example, approximately 0.45% in the 99th percentile of the dense Eastern region. Counties, as a geographic unit, provide a reasonable range and comparable distribution of the child population across China.

Table B.2: The Distribution of the Number of Overlapping Grid Points ($0.25° \times 0.25°$ longitude–latitude grid) and the Distribution of Children (ages 0–14) among the 2369 Chinese Counties in 1990 and 2853 Chinese Counties in 2020

| Number of grid points | Number of counties | | Percentage of children | | Cumulative percentage of children | |
|---|---|---|---|---|---|---|
| | 1990 | 2020 | 1990 | 2020 | 1990 | 2020 |
| **Panel A: Less than 6 grid points falling within a county** | | | | | | |
| 1 | 503 | 957 | 19.89% | 34.51% | 19.89% | 34.51% |
| 2 | 467 | 508 | 21.29% | 20.18% | 41.19% | 54.68% |
| 3 | 378 | 382 | 17.58% | 15.51% | 58.77% | 70.19% |
| 4 | 307 | 309 | 16.08% | 12.94% | 74.84% | 83.13% |
| 5 | 171 | 167 | 8.10% | 6.23% | 82.94% | 89.36% |
| **Panel B: Between 6 and 50 grid points falling within a county** | | | | | | |
| 6 to 10 | 280 | 275 | 12.65% | 7.42% | 95.59% | 96.77% |
| 11 to 20 | 135 | 131 | 2.77% | 1.77% | 98.36% | 98.54% |
| 21 to 30 | 46 | 41 | 0.75% | 0.68% | 99.11% | 99.22% |
| 31 to 40 | 29 | 27 | 0.34% | 0.27% | 99.46% | 99.50% |
| 41 to 50 | 14 | 15 | 0.19% | 0.13% | 99.65% | 99.63% |
| **Panel C: 51 or more grid points falling within a county** | | | | | | |
| 51 to 100 | 24 | 27 | 0.25% | 0.27% | 99.90% | 99.89% |
| 101 to 200 | 12 | 11 | 0.09% | 0.09% | 99.99% | 99.99% |
| 201 to 330 | 3 | 3 | 0.01% | 0.01% | 100.00% | 100.00% |

*Note:* We overlay boundaries for Chinese counties (administrative level 3) in 1990 and 2020 with $0.25° \times 0.25°$ longitude–latitude spatial grids, which is the spatial resolution for the Universal Thermal Climate Index (UTCI) data that we use. We count the number of grid points that intersect (fall within the boundary) with each Chinese county. For county boundaries that do not intersect with points on the grid, we associate the county with the spatial grid point closest to the centroid location of the county, and count that county as having 1 grid point. We assign 127 counties from 1990 and 393 counties from 2020 a grid point due to their lack of intersection. In the first column, we present categorizations of counties by the number of $0.25° \times 0.25°$ spatial grid points. In the second and third columns, we count the number of counties intersecting with different numbers of spatial grid points in 1990 and 2020. In the fourth and fifth columns, we show the percentage of children, as a share of the overall child population (ages 0–14), that reside in the counties categorized in the second and third columns. In the sixth and seventh columns, we show the corresponding cumulative percentage of children. The statistics show, for example, that in 1990, 467 counties intersect with two $0.25° \times 0.25°$ spatial grid points, these counties account for 21.3% of the child population in 1990, and 41.2% of children reside in counties with equal or less than two intersecting UTCI spatial grid points. Panel A, depicting counties intersecting with one to five grid points accounts for approximately 82.9% and 89.4% of cumulative percentage of children in 1990 and 2020 respectively. Less than 20% of children live in counties intersecting with more than five grid points, indicating the county-level as a reasonable measure when assigning UTCI exposure for children.

# C Additional Results on Heat Exposure for Children

Code and results for the additional results in this section as well as in the main text of the paper are accessible at: https://github.com/ClimateInequality/PrjCEC.

## C.1 Shares of Time of Heat Exposure for the Average Child (STAC)

In Tables C.1 and C.2, we present additional details on changes in the average shares of time that Chinese children (ages 0–14) are at risk of heat exposure, between the years 1990 and 2020. Selected STAC results are visualized in Figure 1. We compute the annual average share of time that Chinese children are exposed to UTCI temperatures at or above various thresholds $z\,^{\circ}$C. We group thresholds by panels focusing at least borderline thermal stress (23 °C–25 °C), at least moderate heat stress (26 °C–31 °C), at least strong heat stress (32 °C–37 °C), and very strong heat stress (38 °C–40 °C).

Table C.1's first four columns contain our main results where we consider ambient exposure during all hours of 1990 and 2020. The remaining four columns in Table C.1 present results considering only daytime (between 6 am and 10 pm) hours. Table C.2 presents results where we compare average exposures in the warmer months of April, May, June, July, August, and September with exposures during the colder months of January, February, March, October, November, and December in 1990 and 2020.

Tables C.1 and C.2 show that children's share of time at or above various UTCI heat stress thresholds increased across all heat stress thresholds. Specifically, Tables C.1 and C.2 show that there are between 14 and 18 percent increases the average share of time that children experienced at least moderate and strong heat stress for all hours, daytime hours only, as well as all hours between April and September. Interestingly, despite their low levels (less than 0.5% share of time), Table C.2 shows that heat exposure increased substantially during the colder months by 14% to 476% across thresholds between 1990 and 2020.

Table C.1: Change in Average Share of Time at or above UTCI Heat Thresholds for Chinese Children (ages 0-14), 1990 to 2020

| | All annual hours $\geqslant$ UTCI thresholds | | | | Day time (6 am-10 pm) hours $\geqslant$ UTCI thresholds | | | |
|---|---|---|---|---|---|---|---|---|
| | Share of time | | Changes | | Share of time | | Changes | |
| UTCI thresholds | 1990 | 2020 | Level | % | 1990 | 2020 | Level | % |
| **Panel A: Very strong heat stress** | | | | | | | | |
| $\geqslant 40\,^\circ$C | 0.3% | 0.3% | 0.0007pp | 0.2% | 0.4% | 0.4% | 0.001pp | 0.2% |
| $\geqslant 39\,^\circ$C | 0.6% | 0.6% | 0.0pp | 6.7% | 0.9% | 0.9% | 0.1pp | 6.7% |
| $\geqslant 38\,^\circ$C | 1.0% | 1.2% | 0.1pp | 10.6% | 1.6% | 1.7% | 0.2pp | 10.7% |
| **Panel B: At least strong heat stress** | | | | | | | | |
| $\geqslant 37\,^\circ$C | 1.7% | 1.9% | 0.3pp | 15.1% | 2.5% | 2.9% | 0.4pp | 15.1% |
| $\geqslant 36\,^\circ$C | 2.5% | 2.9% | 0.4pp | 17.3% | 3.7% | 4.4% | 0.6pp | 17.3% |
| $\geqslant 35\,^\circ$C | 3.4% | 4.1% | 0.6pp | 18.1% | 5.2% | 6.1% | 0.9pp | 18.1% |
| $\geqslant 34\,^\circ$C | 4.6% | 5.4% | 0.8pp | 17.5% | 6.8% | 8.0% | 1.2pp | 17.5% |
| $\geqslant 33\,^\circ$C | 5.8% | 6.7% | 0.9pp | 16.1% | 8.7% | 10.1% | 1.4pp | 16.1% |
| $\geqslant 32\,^\circ$C | 7.2% | 8.3% | 1.1pp | 14.7% | 10.8% | 12.3% | 1.6pp | 14.8% |
| **Panel C: At least moderate heat stress** | | | | | | | | |
| $\geqslant 31\,^\circ$C | 8.7% | 9.9% | 1.2pp | 13.9% | 12.9% | 14.7% | 1.8pp | 13.8% |
| $\geqslant 30\,^\circ$C | 10.4% | 11.8% | 1.4pp | 13.6% | 15.2% | 17.3% | 2.0pp | 13.2% |
| $\geqslant 29\,^\circ$C | 12.3% | 14.1% | 1.7pp | 14.0% | 17.7% | 20.0% | 2.3pp | 12.8% |
| $\geqslant 28\,^\circ$C | 14.6% | 16.8% | 2.2pp | 14.8% | 20.4% | 22.9% | 2.6pp | 12.5% |
| $\geqslant 27\,^\circ$C | 17.2% | 19.8% | 2.5pp | 14.8% | 23.2% | 26.0% | 2.8pp | 12.0% |
| $\geqslant 26\,^\circ$C | 20.1% | 22.8% | 2.7pp | 13.5% | 26.2% | 29.1% | 2.9pp | 11.0% |
| **Panel D: At least borderline thermal stress** | | | | | | | | |
| $\geqslant 25\,^\circ$C | 23.0% | 25.7% | 2.7pp | 11.8% | 29.3% | 32.1% | 2.8pp | 9.7% |
| $\geqslant 24\,^\circ$C | 25.9% | 28.6% | 2.6pp | 10.1% | 32.3% | 35.1% | 2.7pp | 8.5% |
| $\geqslant 23\,^\circ$C | 28.7% | 31.3% | 2.6pp | 9.0% | 35.3% | 38.1% | 2.7pp | 7.7% |

*Note:* Columns 1, 2, 5, and 6 show the annual average share of time at or above various UTCI thresholds (UTCI temperatures at $\geqslant z\,^\circ$C) for children in China (ages 0–14). Columns 3, 4, 7, and 8 show 1990 to 2020 changes in percentage points (level) or percentage (%) of the average shares of time at or above UTCI heat thresholds. We consider both all hourly as well as only daytime hourly (between 6 am and 10 am) UTCI temperature data.

Table C.2: Change in Average Share of Time at or above UTCI Heat Thresholds for Chinese Children (ages 0-14), during Warmer and Colder Months, 1990 to 2020

| | April–September hours $\geqslant$ UTCI thresholds | | | | October–March hours $\geqslant$ UTCI thresholds | | | |
|---|---|---|---|---|---|---|---|---|
| | Share of time | | Changes | | Share of time | | Changes | |
| UTCI thresholds | 1990 | 2020 | Level | % | 1990 | 2020 | Level | % |
| **Panel A: Very strong heat stress** | | | | | | | | |
| $\geqslant 40\,^\circ$C | 0.6% | 0.6% | 0.001pp | 0.2% | 0.00002% | 0.00008% | 0.00006pp | 334.3% |
| $\geqslant 39\,^\circ$C | 1.2% | 1.2% | 0.1pp | 6.6% | 0.0001% | 0.0004% | 0.0002pp | 159.0% |
| $\geqslant 38\,^\circ$C | 2.1% | 2.3% | 0.2pp | 10.6% | 0.0004% | 0.002% | 0.001pp | 373.7% |
| **Panel B: At least strong heat stress** | | | | | | | | |
| $\geqslant 37\,^\circ$C | 3.3% | 3.8% | 0.5pp | 14.9% | 0.002% | 0.010% | 0.008pp | 476.0% |
| $\geqslant 36\,^\circ$C | 4.9% | 5.8% | 0.8pp | 17.0% | 0.006% | 0.02% | 0.0pp | 291.4% |
| $\geqslant 35\,^\circ$C | 6.9% | 8.1% | 1.2pp | 17.7% | 0.02% | 0.05% | 0.0pp | 144.1% |
| $\geqslant 34\,^\circ$C | 9.0% | 10.6% | 1.6pp | 17.1% | 0.06% | 0.10% | 0.0pp | 67.0% |
| $\geqslant 33\,^\circ$C | 11.5% | 13.3% | 1.8pp | 15.8% | 0.1% | 0.2% | 0.0pp | 35.1% |
| $\geqslant 32\,^\circ$C | 14.1% | 16.2% | 2.1pp | 14.7% | 0.3% | 0.3% | 0.0pp | 14.1% |
| **Panel C: At least moderate heat stress** | | | | | | | | |
| $\geqslant 31\,^\circ$C | 16.9% | 19.3% | 2.4pp | 14.2% | 0.5% | 0.5% | 0.0pp | 4.2% |
| $\geqslant 30\,^\circ$C | 20.0% | 22.8% | 2.8pp | 14.1% | 0.8% | 0.8% | 0.0pp | 2.5% |
| $\geqslant 29\,^\circ$C | 23.4% | 26.9% | 3.4pp | 14.6% | 1.2% | 1.2% | 0.0pp | 3.0% |
| $\geqslant 28\,^\circ$C | 27.5% | 31.7% | 4.3pp | 15.5% | 1.7% | 1.7% | 0.1pp | 3.4% |
| $\geqslant 27\,^\circ$C | 32.0% | 37.0% | 5.0pp | 15.6% | 2.4% | 2.4% | 0.1pp | 2.8% |
| $\geqslant 26\,^\circ$C | 36.9% | 42.2% | 5.3pp | 14.5% | 3.2% | 3.3% | 0.1pp | 2.5% |
| **Panel D: At least borderline thermal stress** | | | | | | | | |
| $\geqslant 25\,^\circ$C | 41.7% | 47.0% | 5.3pp | 12.7% | 4.2% | 4.4% | 0.1pp | 2.7% |
| $\geqslant 24\,^\circ$C | 46.3% | 51.4% | 5.1pp | 11.0% | 5.4% | 5.6% | 0.2pp | 3.0% |
| $\geqslant 23\,^\circ$C | 50.6% | 55.5% | 4.9pp | 9.7% | 6.8% | 7.1% | 0.3pp | 4.0% |

*Note:* Columns 1, 2, 5, and 6 show the annual average share of time at or above various UTCI thresholds (UTCI temperatures at $\geqslant z\,^\circ$C) for children in China (ages 0–14). Columns 3, 4, 7, and 8 show 1990 to 2020 changes in percentage points (level) or percentage (%) of the average shares of time at or above UTCI heat thresholds. We compare UTCI temperatures in 1990 and 2020 during April, May, June, July, August and September and during January, February, March, October, November and December. We consider all 24 hours.

## C.2 Share of Children Exposed by Heat Intensity and Duration Thresholdsat Risk of Heat Exposure (SEIDT)

In Tables C.3 and C.4, we present additional details from the SEIDT statistics analysis of the share of children at risk of exposure to heat stress thresholds, considering the dual thresholds of intensity (UTCI temperature thresholds $z\,^{\circ}$C) and duration (share of time-in-year thresholds $y$%). Selected results are visualized in Figure 2. In each scenario, the share of children is computed by aggregating the child population from locations (counties) that experienced a particular combination of intensity and duration of exposures. In Table C.3, Panels A and B present shares of children at risk in 1990 and 2020. In Table C.3, Panels A and B present percentage points and percentage changes between 1990 and 2020.

We find that the shares of children experiencing long duration of moderate heat stress increased substantially between 1990 and 2020. In particular, the share of children experiencing at least 3 months of $\geqslant 26\,^{\circ}$C UTCI temperature increased by about one tenth from 31.1% to 34.8%, at least 3 months of $\geqslant 28\,^{\circ}$C UTCI temperature more than doubled from 7.5% to 17.4%, and at least 3 months of $\geqslant 30\,^{\circ}$C UTCI temperature increased by more than six times from 0.4% to 3.0%.

We also find a growing share of children experiencing at least strong and very strong heat stress. In particular, the share of children experiencing $\geqslant 34\,^{\circ}$C UTCI temperature for at least 1.5 months increased by about six times from 0.5% to 3.4%, experiencing $\geqslant 36\,^{\circ}$C UTCI temperature for at least 1 month increased by 23 times from less than 0.1% to 2.1%, and experiencing $\geqslant 38\,^{\circ}$C UTCI temperature for at least 2 weeks increased by 18 times from less than 0.1% to 1.8%.

Finally, not only did more children experience high intensities and long duration of heat exposure in 2020 compared to 1990, children experienced in 2020 new exposure combinations at higher intensities and with longer duration beyond the 1990 frontier. Specifically, in 1990, no children experienced at least 1 month of $\geqslant 38\,^{\circ}$C UTCI temperature, at least 2 months of $\geqslant 34\,^{\circ}$C, or at least 4 months of $\geqslant 30\,^{\circ}$C UTCI heat exposures, but about 0.1%, 0.4%, and 0.1% of children experienced these in 2020, respectively.

Table C.3: Share of Children at Risk of Heat Stress, 1990 to 2020

| | Share of time in year thresholds and corresponding number of weeks | | | | | | | | |
|---|---|---|---|---|---|---|---|---|---|
| | $\geqslant$ 4% | $\geqslant$ 8% | $\geqslant$ 12% | $\geqslant$ 16% | $\geqslant$ 20% | $\geqslant$ 24% | $\geqslant$ 28% | $\geqslant$ 32% | $\geqslant$ 36% |
| UTCI thresholds | 2 weeks | 4 weeks | 6 weeks | 8 weeks | 10 wks | 12 wks | 14 wks | 16 wks | 18 wks |
| **Panel A: 1990** | | | | | | | | | |
| x% (cell) of children with at least y% (column) of time in year 1990 experiencing $\geqslant z$ °C (row) UTCI temperature. | | | | | | | | | |
| **Very strong heat stress** | | | | | | | | | |
| $\geqslant$ 38 °C | 0.1% | | | | | | | | |
| **At least strong heat stress** | | | | | | | | | |
| $\geqslant$ 36 °C | 27.2% | 0.1% | | | | | | | |
| $\geqslant$ 34 °C | 60.1% | 15.1% | 0.5% | | | | | | |
| $\geqslant$ 32 °C | 72.7% | 52.1% | 11.2% | 1.4% | 0.1% | | | | |
| **At least moderate heat stress** | | | | | | | | | |
| $\geqslant$ 30 °C | 80.9% | 69.0% | 43.7% | 13.1% | 4.5% | 0.4% | | | |
| $\geqslant$ 28 °C | 91.4% | 77.5% | 68.0% | 44.6% | 19.5% | 7.5% | 4.5% | 1.4% | 0.1% |
| $\geqslant$ 26 °C | 97.2% | 87.0% | 76.6% | 68.5% | 54.4% | 31.1% | 16.3% | 8.6% | 6.7% |
| **At least borderline thermal stress** | | | | | | | | | |
| $\geqslant$ 24 °C | 98.8% | 96.0% | 84.9% | 76.6% | 70.8% | 63.2% | 44.2% | 25.3% | 13.9% |
| **Panel B: 2020** | | | | | | | | | |
| x% (cell) of children with at least y% (column) of time in year 2020 experiencing $\geqslant z$ °C (row) UTCI temperature. | | | | | | | | | |
| **Very strong heat stress** | | | | | | | | | |
| $\geqslant$ 38 °C | 1.8% | 0.1% | | | | | | | |
| **At least strong heat stress** | | | | | | | | | |
| $\geqslant$ 36 °C | 32.4% | 2.1% | 0.2% | | | | | | |
| $\geqslant$ 34 °C | 66.6% | 20.1% | 3.4% | 0.4% | | | | | |
| $\geqslant$ 32 °C | 77.8% | 59.1% | 18.6% | 6.1% | 0.6% | | | | |
| **At least moderate heat stress** | | | | | | | | | |
| $\geqslant$ 30 °C | 86.0% | 75.6% | 52.9% | 20.7% | 10.4% | 3.0% | 0.5% | 0.1% | |
| $\geqslant$ 28 °C | 94.3% | 83.5% | 74.6% | 53.6% | 25.9% | 17.4% | 10.9% | 7.4% | 3.8% |
| $\geqslant$ 26 °C | 97.7% | 91.9% | 81.4% | 74.5% | 59.7% | 34.8% | 24.9% | 17.9% | 13.7% |
| **At least borderline thermal stress** | | | | | | | | | |
| $\geqslant$ 24 °C | 98.7% | 97.0% | 89.7% | 81.2% | 76.4% | 65.6% | 45.1% | 32.4% | 23.3% |

*Note:* Cells show the shares of Chinese children (ages 0–14) experiencing at least y% of their time in a year to $\geqslant z$ °C UTCI temperature. Shares of children are computed based on aggregating population shares from locations (counties) experiencing the various combinations of heat stress duration (share of time) and intensity (UTCI temperature) thresholds. For shares of time in a year, the correspondence between the share of time and the number of weeks is based on the fact that the average of N weeks of time and $\frac{N}{4}$ months of time is approximately $(N \cdot 2)$% of total share of time in a year. To enhance contrast, values are rounded and cells with values less than 0.05% or 0.05pp are left empty. We consider all 24 hours and 12 months.

Table C.4: Change in Share of Children at Risk of Exposure to Heat Stress Thresholds, 2020–1990

| | Minimal share of time in year thresholds and corresponding number of weeks | | | | | | | | |
|---|---|---|---|---|---|---|---|---|---|
| | $\geqslant$ 4% | $\geqslant$ 8% | $\geqslant$ 12% | $\geqslant$ 16% | $\geqslant$ 20% | $\geqslant$ 24% | $\geqslant$ 28% | $\geqslant$ 32% | $\geqslant$ 36% |
| UTCI thresholds | 2 weeks | 4 weeks | 6 weeks | 8 weeks | 10 wks | 12 wks | 14 wks | 16 wks | 18 wks |
| **Panel a:** 2020% − 1990% | | | | | | | | | |
| Increases in percentage points (cell) of children with at least y% (column) of time at $\geqslant z$ °C (row) heat threshold | | | | | | | | | |
| **Very strong heat stress** | | | | | | | | | |
| $\geqslant$ 38 °C | 1.7pp | 0.1pp | | | | | | | |
| **At least strong heat stress** | | | | | | | | | |
| $\geqslant$ 36 °C | 5.2pp | 2.0pp | 0.2pp | | | | | | |
| $\geqslant$ 34 °C | 6.6pp | 5.0pp | 2.9pp | 0.4pp | | | | | |
| $\geqslant$ 32 °C | 5.1pp | 6.9pp | 7.4pp | 4.7pp | 0.5pp | | | | |
| **At least moderate heat stress** | | | | | | | | | |
| $\geqslant$ 30 °C | 5.2pp | 6.5pp | 9.2pp | 7.6pp | 6.0pp | 2.6pp | 0.5pp | 0.1pp | |
| $\geqslant$ 28 °C | 2.8pp | 6.0pp | 6.6pp | 8.9pp | 6.4pp | 9.9pp | 6.4pp | 6.0pp | 3.8pp |
| $\geqslant$ 26 °C | 0.6pp | 5.0pp | 4.8pp | 6.0pp | 5.2pp | 3.7pp | 8.6pp | 9.3pp | 7.0pp |
| **At least borderline thermal stress** | | | | | | | | | |
| $\geqslant$ 24 °C | -0.2pp | 1.0pp | 4.8pp | 4.6pp | 5.5pp | 2.5pp | 0.9pp | 7.2pp | 9.4pp |
| **Panel b:** $\frac{2020\% - 1990\%}{1990\%} \cdot 100$ | | | | | | | | | |
| Percentage increases (cell) of children with at least y% (column) of time at $\geqslant z$ °C (row) heat threshold | | | | | | | | | |
| **Very strong heat stress** | | | | | | | | | |
| $\geqslant$ 38 °C | 1.8k% | | | | | | | | |
| **At least strong heat stress** | | | | | | | | | |
| $\geqslant$ 36 °C | 19.2% | 2.3k% | | | | | | | |
| $\geqslant$ 34 °C | 10.9% | 33.1% | 606% | | | | | | |
| $\geqslant$ 32 °C | 7.0% | 13.3% | 66.3% | 330% | 792% | | | | |
| **At least moderate heat stress** | | | | | | | | | |
| $\geqslant$ 30 °C | 6.4% | 9.4% | 20.9% | 58.5% | 133% | 654% | | | |
| $\geqslant$ 28 °C | 3.1% | 7.7% | 9.7% | 20.0% | 32.9% | 131% | 141% | 414% | 5.2k% |
| $\geqslant$ 26 °C | 0.6% | 5.7% | 6.3% | 8.7% | 9.6% | 11.7% | 52.9% | 109% | 106% |
| **At least borderline thermal stress** | | | | | | | | | |
| $\geqslant$ 24 °C | -0.2% | 1.0% | 5.7% | 6.0% | 7.8% | 3.9% | 2.1% | 28.5% | 67.5% |

*Note:* Cells show changes between 1990 and 2020 in percentage points (Panel A) and percentage (Panel B) of the shares of Chinese children (ages 0–14) experiencing at least $y$% of their time in a year to $\geqslant z$ °C UTCI temperature. Shares of children are computed based on aggregating population shares from locations (counties) experiencing the various combinations of heat stress duration (share of time) and intensity (UTCI temperature) thresholds. For shares of time in a year, the correspondence between the share of time and the number of weeks is based on the fact that the average of $N$ weeks of time and $\frac{N}{4}$ months of time is approximately $(N \cdot 2)$% of total share of time in a year. To enhance contrast, values are rounded and cells with values less than 0.05% or 0.05pp are left empty. We consider all 24 hours and 12 months.

### C.3 Decomposing Shifts in Population and Temperature Distributions

In Tables C.5 and C.6, we provide details on the relative contributions of shifts in the child population distribution and the UTCI temperature distribution to overall changes in the average shares of time of heat exposure for children. Selected results are visualized in Figure 3. Columns 1–3 of the tables follow from Table C.1. In columns 4–6 of the tables, we use the 1990 population distribution jointly with the 2020 UTCI temperature distribution. In columns 7–9, we consider exposures if the 2020 population distribution faced the 1990 UTCI temperature distribution. Residual unexplained changes are attributed to population and UTCI temperature shift interactions. Our STAC-based decomposition analysis is statistical in nature: We shift one distribution while holding the other constant and do not model mechanisms of change.

In Table C.5, nationally, we show that shifts in the child population distribution between 1990 and 2020 account for 39% to 50% of the increases in the average shares of time of that children are exposed to at least moderate or at least strong heat stress. In contrast, within the Eastern and Northeastern regions, child population distribution shifts account for 5% to 38% of the aggregate regional increases in average child heat exposure. The national results are due to both within- and across-region shifts, whereas the regional results are attributed to only within-region shifts.

In the last column of Tables C.5 we note the decreased importance of population effects in explaining overall changes at higher UTCI thresholds. For example, nationally, the population-shift contributions to overall changes decreased from 61% for at least borderline heat stress ($\geqslant 24\,^{\circ}\mathrm{C}$) to 39% for the upper-bound of at least strong heat stress ($\geqslant 36\,^{\circ}\mathrm{C}$); for the Eastern region, the corresponding numbers decreased from 61% to 19%. These mean that increases at higher heat exposure thresholds come more from increasing UTCI temperatures rather than from populations moving to locations that were already hotter in 1990.

For completeness, in Table C.6, we also present decompositions of regional changes from the Central and Western regions. Child population shifts also help to explain the relatively limited aggregate heat exposures changes in these regions.

Table C.5: Decompose Changes in Average Share of Time Exposed to Heat

| | Actual 2020 vs 1990 | | | 2020 UTCI with 1990 population | | | 1990 UTCI with 2020 population | | |
|---|---|---|---|---|---|---|---|---|---|
| | Share of time | | Changes | Share-time | Decompose changes | | Share-time | Decompose changes | |
| UTCI thresholds | 1990 | 2020 | Δ | Prediction | Vs. 1990 | % of Δ | Prediction | Vs. 1990 | % of Δ |
| **Panel A: National** | | | | | | | | | |
| **At least strong heat stress** | | | | | | | | | |
| $\geqslant 36\,^{\circ}C$ | 2.5% | 2.9% | 0.43pp | 2.7% | 0.17pp | 40% | 2.7% | 0.17pp | 39% |
| $\geqslant 34\,^{\circ}C$ | 4.6% | 5.4% | 0.80pp | 4.9% | 0.35pp | 45% | 4.9% | 0.33pp | 42% |
| $\geqslant 32\,^{\circ}C$ | 7.2% | 8.3% | 1.06pp | 7.6% | 0.44pp | 42% | 7.7% | 0.51pp | 48% |
| **At least moderate heat stress** | | | | | | | | | |
| $\geqslant 30\,^{\circ}C$ | 10.4% | 11.8% | 1.42pp | 11.0% | 0.60pp | 42% | 11.1% | 0.69pp | 49% |
| $\geqslant 28\,^{\circ}C$ | 14.6% | 16.8% | 2.16pp | 15.5% | 0.90pp | 42% | 15.6% | 0.98pp | 45% |
| $\geqslant 26\,^{\circ}C$ | 20.1% | 22.8% | 2.72pp | 21.2% | 1.08pp | 40% | 21.4% | 1.35pp | 50% |
| **At least borderline thermal stress** | | | | | | | | | |
| $\geqslant 24\,^{\circ}C$ | 25.9% | 28.6% | 2.63pp | 26.8% | 0.88pp | 33% | 27.5% | 1.60pp | 61% |
| **Panel B: Eastern region** | | | | | | | | | |
| **At least strong heat stress** | | | | | | | | | |
| $\geqslant 36\,^{\circ}C$ | 2.7% | 3.5% | 0.85pp | 3.3% | 0.59pp | 70% | 2.9% | 0.16pp | 19% |
| $\geqslant 34\,^{\circ}C$ | 5.3% | 6.6% | 1.35pp | 6.1% | 0.89pp | 66% | 5.6% | 0.31pp | 23% |
| $\geqslant 32\,^{\circ}C$ | 8.4% | 10.1% | 1.70pp | 9.5% | 1.03pp | 61% | 8.9% | 0.50pp | 29% |
| **At least moderate heat stress** | | | | | | | | | |
| $\geqslant 30\,^{\circ}C$ | 12.1% | 14.3% | 2.26pp | 13.4% | 1.33pp | 59% | 12.8% | 0.73pp | 32% |
| $\geqslant 28\,^{\circ}C$ | 17.0% | 20.7% | 3.70pp | 19.0% | 2.02pp | 55% | 18.2% | 1.18pp | 32% |
| $\geqslant 26\,^{\circ}C$ | 23.6% | 28.1% | 4.44pp | 25.9% | 2.27pp | 51% | 25.3% | 1.69pp | 38% |
| **At least borderline thermal stress** | | | | | | | | | |
| $\geqslant 24\,^{\circ}C$ | 30.6% | 34.2% | 3.54pp | 32.0% | 1.36pp | 38% | 32.5% | 1.87pp | 53% |
| **Panel C: Northeastern region** | | | | | | | | | |
| **At least strong heat stress** | | | | | | | | | |
| $\geqslant 36\,^{\circ}C$ | 0.04% | 0.3% | 0.27pp | 0.3% | 0.24pp | 89% | 0.05% | 0.01pp | 5% |
| $\geqslant 34\,^{\circ}C$ | 0.3% | 1.1% | 0.79pp | 1.% | 0.72pp | 91% | 0.3% | 0.05pp | 6% |
| $\geqslant 32\,^{\circ}C$ | 1.1% | 2.4% | 1.22pp | 2.3% | 1.12pp | 92% | 1.3% | 0.11pp | 9% |
| **At least moderate heat stress** | | | | | | | | | |
| $\geqslant 30\,^{\circ}C$ | 2.8% | 4.1% | 1.35pp | 4.0% | 1.23pp | 91% | 2.9% | 0.17pp | 13% |
| $\geqslant 28\,^{\circ}C$ | 5.0% | 6.4% | 1.39pp | 6.2% | 1.21pp | 87% | 5.2% | 0.21pp | 15% |
| $\geqslant 26\,^{\circ}C$ | 7.5% | 8.9% | 1.43pp | 8.7% | 1.16pp | 81% | 7.7% | 0.24pp | 16% |
| **At least borderline thermal stress** | | | | | | | | | |
| $\geqslant 24\,^{\circ}C$ | 10.4% | 11.8% | 1.45pp | 11.4% | 1.06pp | 73% | 10.7% | 0.29pp | 20% |

*Note:* Columns (cols) 1–3 include actual annual average share of time that children in China (ages 0–14) are exposed to UTCI temperatures at $\geqslant z\,^{\circ}C$ (same as cols 1–3 in Table C.1). In cols 4–6, the 1990 population distribution face the 2020 UTCI temperature distribution. In cols 7–9, 2020 population face 1990 UTCI temperatures. Cols 4 and 7 show annual average share of time that children are exposed to heat given decomposition scenarios. Cols 5 and 8 show differences between predictions and 1990 actual average shares. Cols 6 and 9 show the share of column 3 actual changes that the predictions from cols 5 and 8 account for. We consider all 24 hours and 12 months.

Table C.6: Decompose Changes in Average Share of Time Exposed to Heat

| | Actual 2020 vs 1990 | | | 2020 UTCI with 1990 population | | | 1990 UTCI with 2020 population | | |
|---|---|---|---|---|---|---|---|---|---|
| | Share of time | | Changes | Share-time | Decompose changes | | Share-time | Decompose changes | |
| UTCI thresholds | 1990 | 2020 | Δ | Prediction | Vs. 1990 | % of Δ | Prediction | Vs. 1990 | % of Δ |
| **Panel A: Central region** | | | | | | | | | |
| **At least strong heat stress** | | | | | | | | | |
| $\geqslant 36\,^{\circ}C$ | 3.7% | 3.7% | 0.08pp | 3.6% | -0.03pp | -33% | 3.7% | 0.02pp | 27% |
| $\geqslant 34\,^{\circ}C$ | 6.2% | 6.5% | 0.25pp | 6.4% | 0.11pp | 45% | 6.3% | 0.03pp | 14% |
| $\geqslant 32\,^{\circ}C$ | 9.3% | 9.6% | 0.30pp | 9.4% | 0.13pp | 43% | 9.3% | 0.04pp | 14% |
| **At least moderate heat stress** | | | | | | | | | |
| $\geqslant 30\,^{\circ}C$ | 12.9% | 13.3% | 0.39pp | 13.1% | 0.21pp | 53% | 12.9% | 0.04pp | 10% |
| $\geqslant 28\,^{\circ}C$ | 17.6% | 17.9% | 0.38pp | 17.8% | 0.19pp | 51% | 17.6% | 0.03pp | 9% |
| $\geqslant 26\,^{\circ}C$ | 23.4% | 23.6% | 0.21pp | 23.4% | 0.04pp | 22% | 23.4% | 0.04pp | 21% |
| **At least borderline thermal stress** | | | | | | | | | |
| $\geqslant 24\,^{\circ}C$ | 29.2% | 29.6% | 0.42pp | 29.5% | 0.27pp | 64% | 29.3% | 0.08pp | 19% |
| **Panel B: Western region** | | | | | | | | | |
| **At least strong heat stress** | | | | | | | | | |
| $\geqslant 36\,^{\circ}C$ | 1.7% | 1.7% | -0.04pp | 1.6% | -0.12pp | 284% | 1.7% | 0.05pp | -112% |
| $\geqslant 34\,^{\circ}C$ | 3.2% | 3.3% | 0.03pp | 3.2% | -0.09pp | -312% | 3.4% | 0.10pp | 345% |
| $\geqslant 32\,^{\circ}C$ | 5.4% | 5.4% | 0.07pp | 5.3% | -0.09pp | -133% | 5.5% | 0.16pp | 247% |
| **At least moderate heat stress** | | | | | | | | | |
| $\geqslant 30\,^{\circ}C$ | 8.0% | 8.2% | 0.19pp | 8.1% | 0.01pp | 7% | 8.2% | 0.19pp | 102% |
| $\geqslant 28\,^{\circ}C$ | 11.5% | 12.1% | 0.52pp | 11.8% | 0.29pp | 55% | 11.8% | 0.24pp | 47% |
| $\geqslant 26\,^{\circ}C$ | 16.2% | 17.2% | 1.06pp | 16.9% | 0.77pp | 73% | 16.5% | 0.30pp | 28% |
| **At least borderline thermal stress** | | | | | | | | | |
| $\geqslant 24\,^{\circ}C$ | 21.5% | 22.7% | 1.13pp | 22.4% | 0.91pp | 81% | 21.8% | 0.30pp | 26% |

*Note:* Columns (cols) 1–3 include actual annual average share of time that children in the Central and Western regions of China (ages 0–14) are exposed to UTCI temperatures at $\geqslant z\,^{\circ}C$ (same as cols 1–3 in Table C.1). In cols 4–6, the 1990 population distribution face the 2020 UTCI temperature distribution. In cols 7–9, 2020 population face 1990 UTCI temperatures. Cols 4 and 7 show annual average share of time that children are exposed to heat given decomposition scenarios. Cols 5 and 8 show differences between predictions and 1990 actual average shares. Cols 6 and 9 show the share of column 3 actual changes that the predictions from cols 5 and 8 account for. We consider all 24 hours and 12 months.

## C.4 Additional Regional Analysis

In Tables C.7 and C.8, we present details on region- and province-specific STAC child heat exposure analysis. Selected regional results are visualized in Figure 4. Sub-national analyses show which areas have experienced greater changes in heat exposures and also shed light on whether aggregate changes are due to population shifts across provinces within regions or across regions.[C.1] Table C.7 presents results for at least strong and very strong heat stress and Table C.8 focuses on at least moderate heat stress.

Between 1990 and 2020, while Central (C) and Western (W) heat exposures stagnated, children in the heated Eastern (E) and colder Northeastern (NE) regions experienced increases of 19%–35% and 19%–7.4k% in average heat exposure time. In 2020, the average E, NE, C, and W region child experienced 10.1%, 2.4%, 9.5%, and 5.4% of her time under at least strong (UTCI $\geqslant 32\,^{\circ}\mathrm{C}$) heat stress.

In 2020, we find that children in Hainan (E), Guangdong (E), Guangxi (W), Jiangxi (C), and Fujian (E) had the highest heat exposures with 19.2%, 15.2%, 13.2%, 12.8%, and 11.8% of their average shares of time exposed to at least strong heat stress (UTCI $\geqslant 32\,^{\circ}\mathrm{C}$), which represented respective increases of 17%, 20%, 8%, 16%, and 54% compared to 1990.

Lastly, we note the importance of considering both changes and levels. While Hebei (E), Zhejiang (E) and NE provinces experienced similar percentage point increases in the average share of heat exposure time, the percentage increases in the NE provinces are 3 to 15 times larger due to lower starting levels. Additionally, Hebei (E) and Jiangsu (E) arrived at similar levels of average child heat exposure in 2020 with a 17% increase and an 11% reduction in average share of heat exposure time, respectively. Locations with similar levels or changes of exposure might require different societal and physical adjustments depending on prior levels and the magnitudes of recent changes.

C.1. Even when there are no changes in UTCI temperatures and within-region population distributions, average national child exposure could increase due to shifts in child population to hotter regions.

Table C.7: Regional Average Share of Time at Risk of Exposure to at least **Strong and Very Strong** Heat Stress Thresholds for Children (ages 0-14), 1990 to 2020

| | At least strong heat stress | | | | | | | | Very strong heat stress | | | |
|---|---|---|---|---|---|---|---|---|---|---|---|---|
| | ⩾ UTCI 32° C | | | | ⩾ UTCI 35° C | | | | ⩾ UTCI 38° C | | | |
| | Share of time | | Changes | | Share of time | | Changes | | Share of time | | Changes | |
| Location | 1990 | 2020 | Level | % | 1990 | 2020 | Level | % | 1990 | 2020 | Level | % |
| **Panel A: Regions** | | | | | | | | | | | | |
| Eastern | 8.4% | 10.1% | 1.7pp | 20% | 3.9% | 5.0% | 1.1pp | 29% | 1.0% | 1.4% | 0.4pp | 35% |
| Northeastern | 1.1% | 2.4% | 1.2pp | 106% | 0.1% | 0.6% | 0.5pp | 457% | 0.0% | 0.1% | 0.1pp | 7.4k% |
| Central | 9.3% | 9.6% | 0.3pp | 3% | 4.9% | 5.1% | 0.2pp | 4% | 1.7% | 1.6% | -0.1pp | -3% |
| Western | 5.4% | 5.4% | 0.1pp | 1% | 2.4% | 2.4% | 0.0pp | 0% | 0.7% | 0.6% | -0.1pp | -18% |
| **Panel B: Eastern region** | | | | | | | | | | | | |
| Beijing | 2.9% | 6.3% | 3.4pp | 117% | 0.5% | 2.8% | 2.3pp | 424% | 0.0% | 0.6% | 0.6pp | 1.2k% |
| Fujian | 7.7% | 11.8% | 4.1pp | 54% | 2.9% | 5.6% | 2.7pp | 94% | 0.5% | 1.3% | 0.9pp | 175% |
| Guangdong | 12.7% | 15.2% | 2.5pp | 20% | 5.7% | 7.5% | 1.8pp | 31% | 1.3% | 2.0% | 0.7pp | 56% |
| Hainan | 16.3% | 19.2% | 2.8pp | 17% | 6.4% | 10.0% | 3.6pp | 57% | 0.9% | 3.4% | 2.4pp | 261% |
| Hebei | 6.5% | 7.6% | 1.1pp | 17% | 2.9% | 3.9% | 1.0pp | 34% | 0.8% | 1.0% | 0.2pp | 31% |
| Jiangsu | 8.7% | 7.8% | -0.9pp | -11% | 4.7% | 3.8% | -0.9pp | -20% | 1.7% | 1.3% | -0.4pp | -25% |
| Shandong | 6.8% | 7.1% | 0.4pp | 6% | 2.9% | 3.3% | 0.4pp | 13% | 0.5% | 0.9% | 0.3pp | 58% |
| Shanghai | 6.8% | 6.1% | -0.7pp | -10% | 3.1% | 2.7% | -0.4pp | -14% | 1.0% | 0.6% | -0.4pp | -40% |
| Tianjin | 5.6% | 7.3% | 1.7pp | 31% | 2.1% | 3.8% | 1.7pp | 84% | 0.2% | 0.9% | 0.7pp | 308% |
| Zhejiang | 8.2% | 9.2% | 1.0pp | 12% | 4.6% | 4.9% | 0.4pp | 8% | 1.9% | 1.6% | -0.3pp | -14% |
| **Panel C: Northeastern region** | | | | | | | | | | | | |
| Heilongjiang | 0.6% | 1.7% | 1.1pp | 175% | 0.0% | 0.4% | 0.4pp | 1.6k% | 0.0% | 0.0% | 0.0pp | |
| Jilin | 0.8% | 2.1% | 1.3pp | 148% | 0.0% | 0.5% | 0.5pp | 2.7k% | 0.0% | 0.0% | 0.0pp | |
| Liaoning | 1.9% | 2.9% | 1.1pp | 56% | 0.3% | 0.8% | 0.6pp | 216% | 0.0% | 0.1% | 0.1pp | 4.5k% |
| **Panel D: Central region** | | | | | | | | | | | | |
| Anhui | 10.1% | 9.3% | -0.8pp | -7% | 5.8% | 5.0% | -0.9pp | -15% | 2.2% | 1.8% | -0.4pp | -18% |
| Henan | 8.9% | 9.5% | 0.6pp | 7% | 4.5% | 5.1% | 0.5pp | 12% | 1.4% | 1.6% | 0.2pp | 13% |
| Hubei | 10.2% | 9.3% | -0.9pp | -9% | 5.5% | 4.9% | -0.6pp | -10% | 2.0% | 1.3% | -0.7pp | -35% |
| Hunan | 10.2% | 10.6% | 0.4pp | 4% | 5.0% | 5.4% | 0.4pp | 7% | 1.6% | 1.6% | 0.0pp | 0% |
| Jiangxi | 11.0% | 12.8% | 1.8pp | 16% | 6.1% | 7.4% | 1.2pp | 20% | 2.4% | 2.9% | 0.5pp | 19% |
| Shanxi | 2.6% | 2.8% | 0.1pp | 5% | 0.8% | 0.7% | -0.1pp | -18% | 0.2% | 0.1% | -0.1pp | -53% |
| **Panel E: Western region** | | | | | | | | | | | | |
| Gansu | 0.8% | 0.8% | 0.0pp | -1% | 0.1% | 0.1% | 0.0pp | -17% | 0.0% | 0.0% | 0.0pp | -17% |
| Guangxi | 12.3% | 13.2% | 1.0pp | 8% | 5.5% | 6.6% | 1.1pp | 20% | 1.5% | 1.4% | -0.1pp | -7% |
| Guizhou | 2.8% | 2.1% | -0.7pp | -26% | 0.7% | 0.3% | -0.4pp | -53% | 0.1% | 0.0% | 0.0pp | -54% |
| Neimenggu | 0.9% | 2.0% | 1.1pp | 116% | 0.1% | 0.6% | 0.4pp | 296% | 0.0% | 0.1% | 0.1pp | 268% |
| Ningxia | 2.1% | 2.8% | 0.7pp | 31% | 0.7% | 0.9% | 0.2pp | 35% | 0.1% | 0.1% | 0.0pp | 17% |
| Qinghai | 0.0% | 0.0% | 0.0pp | | 0.0% | 0.0% | 0.0pp | | 0.0% | 0.0% | 0.0pp | |

*Continued on next page*

Table C.7: Regional Average Share of Time at Risk of Exposure to at least **Strong and Very Strong** Heat Stress Thresholds for Children (ages 0-14), 1990 to 2020

| | At least strong heat stress | | | | | | | | Very strong heat stress | | | |
|---|---|---|---|---|---|---|---|---|---|---|---|---|
| | ⩾ UTCI 32° C | | | | ⩾ UTCI 35° C | | | | ⩾ UTCI 38° C | | | |
| | Share of time | | Changes | | Share of time | | Changes | | Share of time | | Changes | |
| Location | 1990 | 2020 | Level | % | 1990 | 2020 | Level | % | 1990 | 2020 | Level | % |
| Shaanxi | 4.6% | 4.3% | -0.4pp | -8% | 1.9% | 1.5% | -0.4pp | -23% | 0.6% | 0.2% | -0.3pp | -58% |
| Sichuan | 8.0% | 7.4% | -0.7pp | -8% | 4.2% | 3.6% | -0.6pp | -14% | 1.3% | 1.0% | -0.3pp | -23% |
| Xinjiang | 4.3% | 5.2% | 0.9pp | 22% | 2.0% | 2.4% | 0.4pp | 19% | 0.7% | 0.7% | 0.0pp | 0% |
| Xizang | 0.0% | 0.0% | 0.0pp | | 0.0% | 0.0% | 0.0pp | | 0.0% | 0.0% | 0.0pp | |
| Yunnan | 0.9% | 1.2% | 0.3pp | 33% | 0.1% | 0.1% | 0.0pp | 53% | 0.0% | 0.0% | 0.0pp | -7% |

*Note:* We present similar statistics as in Table C.1, but now compute exposures separately for the four economic regions and provincial-level administrative units in China. Columns (cols) 1–3 and 4–6 focus on at least strong UTCI heat exposure at ⩾ 32 °C and ⩾ 35 °C, respectively. Cols 7–9 focus on very strong UTCI heat exposure at ⩾ 38 °C. Cols 1 and 2, 5 and 6, and 9 and 10 show the annual average share of time at or above various UTCI thresholds (UTCI temperatures at ⩾ $z$ °C) for children in China (ages 0–14). Cols 3 and 4, 7 and 8, and 11 and 12 show 1990 to 2020 changes in percentage points (level) or percentage (%) of the average shares of time at or above UTCI heat thresholds. Cells are empty for percentage changes when the denominator is equal to zero. We consider all 24 hours and 12 months.

Table C.8: Regional Average Share of Time at Risk of Exposure to at Least **Moderate** Heat Stress Thresholds for Children (ages 0-14), 1990 to 2020

| | At least borderline thermal stress | | | | At least moderate heat stress | | | | | | | |
|---|---|---|---|---|---|---|---|---|---|---|---|---|
| | ⩾ UTCI 23° C | | | | ⩾ UTCI 26° C | | | | ⩾ UTCI 29° C | | | |
| | Share of time | | Changes | | Share of time | | Changes | | Share of time | | Changes | |
| Location | 1990 | 2020 | Level | % | 1990 | 2020 | Level | % | 1990 | 2020 | Level | % |
| **Panel A: Regions** | | | | | | | | | | | | |
| Eastern | 33.8% | 37.0% | 3.2pp | 9% | 23.6% | 28.1% | 4.4pp | 19% | 14.3% | 17.1% | 2.8pp | 20% |
| Northeastern | 12.0% | 13.5% | 1.5pp | 13% | 7.5% | 8.9% | 1.4pp | 19% | 3.8% | 5.2% | 1.4pp | 36% |
| Central | 32.0% | 32.7% | 0.7pp | 2% | 23.4% | 23.6% | 0.2pp | 1% | 15.1% | 15.5% | 0.4pp | 3% |
| Western | 24.3% | 25.3% | 1.0pp | 4% | 16.2% | 17.2% | 1.1pp | 7% | 9.7% | 10.0% | 0.3pp | 3% |
| **Panel B: Eastern region** | | | | | | | | | | | | |
| Beijing | 19.0% | 23.2% | 4.3pp | 23% | 12.1% | 16.2% | 4.1pp | 34% | 7.0% | 10.7% | 3.7pp | 53% |
| Fujian | 38.9% | 45.6% | 6.7pp | 17% | 24.6% | 32.5% | 7.9pp | 32% | 14.1% | 19.0% | 4.9pp | 35% |
| Guangdong | 51.9% | 55.5% | 3.7pp | 7% | 37.5% | 45.3% | 7.8pp | 21% | 21.6% | 26.3% | 4.7pp | 22% |
| Hainan | 63.5% | 63.4% | 0.0pp | 0% | 47.1% | 51.8% | 4.7pp | 10% | 27.7% | 31.5% | 3.9pp | 14% |
| Hebei | 24.4% | 25.1% | 0.7pp | 3% | 17.0% | 18.0% | 1.0pp | 6% | 10.8% | 12.3% | 1.5pp | 14% |
| Jiangsu | 30.5% | 29.7% | -0.8pp | -3% | 22.5% | 21.5% | -1.0pp | -4% | 14.3% | 13.7% | -0.6pp | -4% |
| Shandong | 26.7% | 25.3% | -1.4pp | -5% | 18.1% | 18.2% | 0.0pp | 0% | 11.4% | 12.1% | 0.7pp | 6% |
| Shanghai | 27.9% | 29.7% | 1.8pp | 7% | 19.7% | 20.7% | 1.0pp | 5% | 12.3% | 11.3% | -1.0pp | -8% |
| Tianjin | 23.5% | 25.2% | 1.7pp | 7% | 15.8% | 17.8% | 1.9pp | 12% | 9.7% | 12.1% | 2.3pp | 24% |
| Zhejiang | 33.4% | 36.0% | 2.6pp | 8% | 22.6% | 26.5% | 3.9pp | 17% | 13.6% | 15.4% | 1.8pp | 13% |

*Continued on next page*

Table C.8: Regional Average Share of Time at Risk of Exposure to at Least **Moderate** Heat Stress Thresholds for Children (ages 0-14), 1990 to 2020

| | At least borderline thermal stress | | | | At least moderate heat stress | | | | | | | |
|---|---|---|---|---|---|---|---|---|---|---|---|---|
| | ⩾ UTCI 23° C | | | | ⩾ UTCI 26° C | | | | ⩾ UTCI 29° C | | | |
| | Share of time | | Changes | | Share of time | | Changes | | Share of time | | Changes | |
| Location | 1990 | 2020 | Level | % | 1990 | 2020 | Level | % | 1990 | 2020 | Level | % |
| **Panel C: Northeastern region** | | | | | | | | | | | | |
| Heilongjiang | 10.2% | 11.2% | 1.0pp | 9% | 6.3% | 7.3% | 0.9pp | 15% | 2.9% | 4.0% | 1.1pp | 38% |
| Jilin | 11.1% | 12.2% | 1.1pp | 10% | 6.9% | 8.5% | 1.5pp | 22% | 3.4% | 4.9% | 1.5pp | 45% |
| Liaoning | 14.4% | 15.8% | 1.4pp | 10% | 9.1% | 10.3% | 1.3pp | 14% | 5.1% | 6.2% | 1.1pp | 21% |
| **Panel D: Central region** | | | | | | | | | | | | |
| Anhui | 32.7% | 32.3% | -0.4pp | -1% | 25.2% | 23.4% | -1.8pp | -7% | 16.2% | 15.5% | -0.7pp | -5% |
| Henan | 29.6% | 29.4% | -0.2pp | -1% | 21.5% | 21.1% | -0.4pp | -2% | 13.9% | 14.5% | 0.6pp | 4% |
| Hubei | 33.3% | 33.9% | 0.6pp | 2% | 25.1% | 24.2% | -0.9pp | -3% | 16.7% | 15.4% | -1.3pp | -8% |
| Hunan | 36.2% | 37.6% | 1.4pp | 4% | 25.7% | 26.8% | 1.1pp | 4% | 16.5% | 17.1% | 0.5pp | 3% |
| Jiangxi | 38.8% | 41.8% | 3.0pp | 8% | 28.1% | 31.7% | 3.6pp | 13% | 17.9% | 20.9% | 3.1pp | 17% |
| Shanxi | 16.1% | 16.6% | 0.5pp | 3% | 10.6% | 11.1% | 0.6pp | 5% | 6.0% | 6.6% | 0.5pp | 9% |
| **Panel E: Western region** | | | | | | | | | | | | |
| Gansu | 11.1% | 10.7% | -0.4pp | -3% | 6.6% | 6.4% | -0.2pp | -3% | 3.0% | 2.9% | 0.0pp | -1% |
| Guangxi | 47.5% | 49.2% | 1.7pp | 4% | 33.3% | 36.8% | 3.4pp | 10% | 20.2% | 21.4% | 1.2pp | 6% |
| Guizhou | 19.5% | 19.4% | -0.1pp | 0% | 12.2% | 11.6% | -0.6pp | -5% | 7.0% | 6.1% | -0.9pp | -13% |
| Neimenggu | 9.9% | 12.0% | 2.1pp | 21% | 6.0% | 8.2% | 2.2pp | 36% | 2.9% | 4.7% | 1.8pp | 62% |
| Ningxia | 12.9% | 14.1% | 1.1pp | 9% | 8.8% | 9.6% | 0.8pp | 10% | 5.0% | 5.7% | 0.7pp | 13% |
| Qinghai | 4.9% | 3.8% | -1.1pp | -23% | 1.4% | 1.0% | -0.4pp | -30% | 0.1% | 0.0% | -0.1pp | -71% |
| Shaanxi | 19.5% | 19.3% | -0.2pp | -1% | 13.3% | 13.1% | -0.3pp | -2% | 8.6% | 8.2% | -0.3pp | -4% |
| Sichuan | 28.5% | 29.4% | 0.8pp | 3% | 19.3% | 19.7% | 0.4pp | 2% | 12.5% | 12.2% | -0.3pp | -3% |
| Xinjiang | 16.3% | 18.0% | 1.6pp | 10% | 11.4% | 13.1% | 1.7pp | 14% | 7.4% | 8.8% | 1.4pp | 18% |
| Xizang | 1.3% | 1.4% | 0.1pp | 5% | 0.1% | 0.1% | 0.0pp | -32% | 0.0% | 0.0% | 0.0pp | 159% |
| Yunnan | 19.2% | 21.0% | 1.8pp | 9% | 11.0% | 12.3% | 1.3pp | 12% | 4.6% | 5.3% | 0.8pp | 17% |

*Note:* We present similar statistics as in Table C.1, but now compute exposures separately for the four economic regions and provincial-level administrative units in China. Columns (cols) 4–6 and 7–9 focus on at least moderate UTCI heat exposure at ⩾ 26 °C and ⩾ 29 °C, respectively. Cols 1–3 provide UTCI heat exposure at ⩾ 23 °C—UTCI 23 °C is a temperature level that is just below the UTCI 25 °C threshold for moderate heat stress. Cols 1 and 2, 5 and 6, and 9 and 10 show the annual average share of time at or above various UTCI thresholds (UTCI temperatures at ⩾ z °C) for children in China (ages 0–14). Cols 3 and 4, 7 and 8, and 11 and 12 show 1990 to 2020 changes in percentage points (level) or percentage (%) of the average shares of time at or above UTCI heat thresholds. Cells are empty for percentage changes when the denominator is equal to zero. We consider all 24 hours and 12 months.

### C.5 Main and Additional Results Replication

Code and results for the additional results in this section as well as in the main text of the paper are accessible at: https://github.com/ClimateInequality/PrjCEC.

Code for generating the statistics shown in tables and figures are stored in the R-script folder, and code and output for visualizaing and tabularization are stored in the res folder.

1. Section C.1 and main text Figure 1 results and code:
    - Generate statistics: R-script/run_1a_mean_child_all24, R-script/run_1b_mean_child_6t22, and R-script/run_1c_mean_child_seasons
    - Tabulate and visualize: R-script/tabfig_1_mean_child
    - Tables and figures: res/res_mean_child
2. Section C.2 and main text Figure 2 results and code:
    - Generate statistics: R-script/run_2a_atrisk_child
    - Tabulate and visualize: R-script/tabfig_2_at_risk
    - Tables and figures: res/res_atrisk
3. Section C.3 and main text Figure 3 results and code:
    - Generate statistics: R-script/run_3a_decompose and R-script/run_3b_decompose_regional
    - Tabulate and visualize: R-script/tabfig_3_decompose
    - Tables and figures: res/res_decompose
4. Section C.4 and main text Figure 4 results and code:
    - Generate statistics: R-script/run_4a_mean_child_all24_by_region and R-script/run_4b_mean_child_all24_by_province
    - Tabulate and visualize: R-script/tabfig_4_region_prov
    - Tables and figures: res/res_region_prov